Article

Chemistry & Biology

Repurposing Hsp104 to Antagonize Seminal Amyloid and Counter HIV Infection

Graphical Abstract

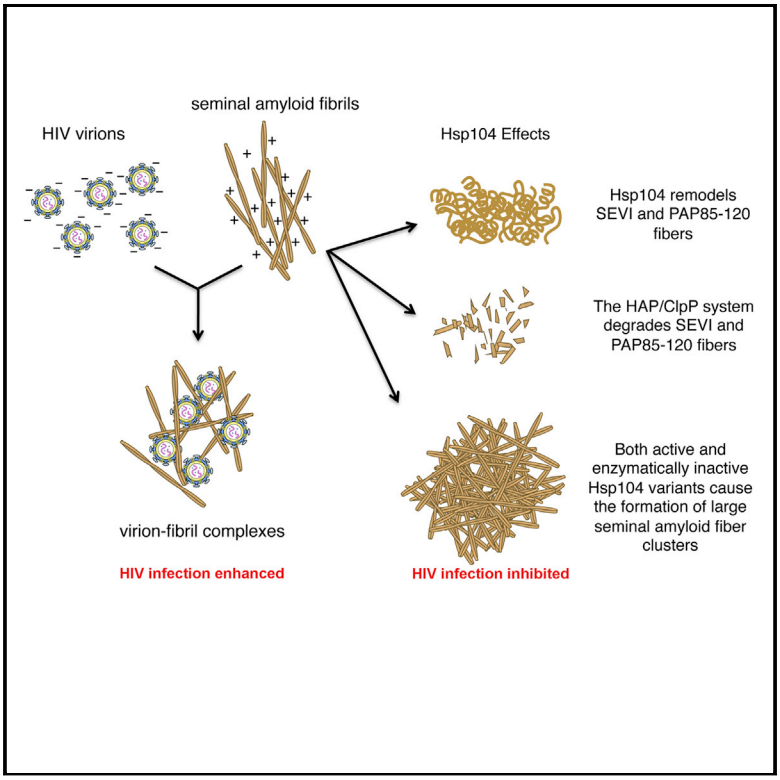

Highlights

- Hsp104 and Hsp104^{A503V} remodel SEVI and PAP85-120 fibrils into non-amyloid forms
- Inactive Hsp104 scaffolds cluster seminal amyloid fibrils into large conglomerates
- HAP plus ClpP remodel and degrade SEVI and PAP85-120 fibrils
- These strategies diminish the ability of seminal amyloid to promote HIV infection

Authors

Laura M. Castellano, Stephen M. Bart, Veronica M. Holmes, Drew Weissman, James Shorter

Correspondence

jshorter@mail.med.upenn.edu

In Brief

Castellano et al. design three disruptive technologies to rapidly antagonize seminal amyloid and reduce its ability to promote HIV infection by repurposing Hsp104, an amyloid-remodeling nanomachine from yeast.

Castellano et al., 2015, Chemistry & Biology 22, 1074–1086
August 20, 2015
http://dx.doi.org/10.1016/j.chembiol.2015.07.007

CellPress

Chemistry & Biology
Article

Repurposing Hsp104 to Antagonize Seminal Amyloid and Counter HIV Infection

Laura M. Castellano,[1,2] Stephen M. Bart,[1,3] Veronica M. Holmes,[4] Drew Weissman,[4] and James Shorter[1,2,3,*]
[1]Department of Biochemistry and Biophysics, Perelman School of Medicine, University of Pennsylvania, Philadelphia, PA 19104, USA
[2]Pharmacology Graduate Group, Perelman School of Medicine, University of Pennsylvania, Philadelphia, PA 19104, USA
[3]Cell and Molecular Biology Graduate Group, Perelman School of Medicine, University of Pennsylvania, Philadelphia, PA 19104, USA
[4]Division of Infectious Diseases, Department of Medicine, Perelman School of Medicine, University of Pennsylvania, Philadelphia, PA 19104, USA
*Correspondence: jshorter@mail.med.upenn.edu
http://dx.doi.org/10.1016/j.chembiol.2015.07.007

SUMMARY

Naturally occurring proteolytic fragments of prostatic acid phosphatase (PAP248-286 and PAP85-120) and semenogelins (SEM1 and SEM2) form amyloid fibrils in seminal fluid, which capture HIV virions and promote infection. For example, PAP248-286 fibrils, termed SEVI (semen-derived enhancer of viral infection), can potentiate HIV infection by several orders of magnitude. Here, we design three disruptive technologies to rapidly antagonize seminal amyloid by repurposing Hsp104, an amyloid-remodeling nanomachine from yeast. First, Hsp104 and an enhanced engineered variant, Hsp104^{A503V}, directly remodel SEVI and PAP85-120 fibrils into non-amyloid forms. Second, we elucidate catalytically inactive Hsp104 scaffolds that do not remodel amyloid structure, but cluster SEVI, PAP85-120, and SEM1(45–107) fibrils into larger assemblies. Third, we modify Hsp104 to interact with the chambered protease ClpP, which enables coupled remodeling and degradation to irreversibly clear SEVI and PAP85-120 fibrils. Each strategy diminished the ability of seminal amyloid to promote HIV infection, and could have therapeutic utility.

INTRODUCTION

HIV is a global epidemic that has killed nearly 30 million people since its discovery (UNAIDS, 2010). The HIV pandemic is most severe in the developing world. In Sub-Saharan Africa, ~5% of adults are infected with the virus (UNAIDS, 2011). Nearly 80% of HIV infections are acquired through heterosexual transmission (Gray et al., 2001; Pilcher et al., 2004; Royce et al., 1997), and endogenous peptides in semen play a critical role in the spread of this retrovirus (Arnold et al., 2012; Münch et al., 2007; Roan et al., 2011).

Naturally occurring fragments of proteins abundant in semen form amyloid fibrils (Usmani et al., 2014), and the unique composition of semen drives the fibrillization process (Olsen et al., 2012). Specifically, proteolytic fragments of prostatic acid phosphatase (PAP248-286 [SEVI] and PAP85-120), semenogelin 1 (SEM1), and semenogelin 2 (SEM2) form fibrils that enhance HIV infectivity by several orders of magnitude under conditions of limiting viral inoculum, whereas the soluble, non-amyloid peptides have no effect (Arnold et al., 2012; Münch et al., 2007; Roan et al., 2011). Polylysine and other cationic polymers such as polybrene can enhance HIV infection in cell culture, but are not as effective at low concentrations as SEVI fibrils (Münch et al., 2007; Sievers et al., 2011; Yolamanova et al., 2013). Semen-derived fibrils are highly basic and contain a large proportion of lysine and arginine residues. These charged fibrils promote HIV infection by neutralizing the inherent electrostatic repulsion between the negatively charged surfaces of HIV virions and target cells, and, through direct binding to virions, fibrils simultaneously promote viral binding to the cell surface (Roan et al., 2009). Amyloid fibrils are implicated in numerous neurodegenerative and systemic diseases, and they are notoriously difficult to clear due to their self-templating character and stability, which lies at the extremes of protein-based structures (Knowles et al., 2014). Nonetheless, eliminating semen-derived fibrils could massively reduce viral transmission (Castellano and Shorter, 2012). This approach could be advantageous because it targets host-encoded viral-enhancing factors rather than the viral machinery itself. However, because diverse polypeptides form fibrils in semen that promote viral infection, we explored remodeling factors with activity against diverse amyloids, rather than agents with specialized activity against any single peptide (Castellano and Shorter, 2012; Sievers et al., 2011).

With this design principle in mind, we turned to Hsp104, an amyloid-remodeling nanomachine and AAA+ protein (Shorter, 2008). Hsp104 renatures amorphous protein aggregates following thermal or chemical stress, and catalytically deconstructs diverse amyloid fibrils (DeSantis et al., 2012; Glover and Lindquist, 1998; Jackrel et al., 2014; Klaips et al., 2014; Liu et al., 2011; Lo Bianco et al., 2008; Shorter and Lindquist, 2004, 2006). Hsp104 is a generalist, and is adapted to remodel diverse prion conformers and disaggregate a large proportion of the yeast proteome in response to environmental stress (Vashist et al., 2010). Despite being highly conserved in eubacteria and eukaryotes, Hsp104 homologs are absent in metazoa (Shorter, 2008). However, Hsp104 has previously been utilized in metazoan systems to counteract disease-associated protein aggregates and amyloid fibrils (Cushman-Nick et al., 2013; Kim et al., 2013; Lo Bianco et al., 2008; Vashist et al., 2010).

Here, we exploit the broad-spectrum, amyloid-remodeling activity of Hsp104 to antagonize semen-derived amyloid fibrils and reduce HIV transmission. We devise three disruptive technologies to antagonize seminal amyloid based on Hsp104. Our findings provide insight into developing nanomachines to abolish the infection-enhancing capabilities of seminal amyloid and complementing microbicidal approaches.

RESULTS

Hsp104 Remodels SEVI Fibrils

First, we tested whether Hsp104 can remodel SEVI fibrils. We assessed fibril remodeling using the amyloid-binding dye, Thioflavin-T (ThT), and by transmission electron microscopy (TEM). Incubation of SEVI fibrils with a substoichiometric concentration of Hsp104 (PAP248-286:Hsp104 of 6.67:1) reduced ThT fluorescence intensity to ~37% of the initial value after 2 hr, and a further decrease to ~27% was observed after 6 hr (Figure 1A). The ThT fluorescence intensity plateaued after 6 hr, indicating that amyloid fibrils cannot reform rapidly after Hsp104-mediated remodeling. Hsp104 remodels SEVI fibrils more rapidly than the green tea polyphenol, epigallocatechin-3-gallate, which slowly eradicates SEVI fibrils over the course of 24–48 hr (Hauber et al., 2009). TEM revealed that the products of Hsp104 remodeling were structures resembling amorphous protein aggregates (Figure 1B). After 2 hr, SEVI fibrils were completely converted into these non-amyloid aggregates by Hsp104, and no further alteration in morphology was observed after 24 hr. Dose-response analysis of Hsp104-mediated remodeling of SEVI fibrils indicates a half-maximal effective concentration (EC_{50}) value of ~0.72 μM (Figure 1C).

We obtained a similar result when SEVI fibrils were incubated with Hsp104 plus Hsp70 and Hsp40. Hsp70 and Hsp40 are usually required for disaggregation of amorphous protein aggregates by Hsp104, whereas amyloid remodeling by Hsp104 does not always necessitate Hsp70 and Hsp40 (DeSantis et al., 2012; Glover and Lindquist, 1998; Shorter and Lindquist, 2004, 2006, 2008). However, in some instances Hsp70 and Hsp40 can enhance Hsp104-mediated disassembly of amyloid (DeSantis et al., 2012; DeSantis and Shorter, 2012b; Lo Bianco et al., 2008; Shorter, 2011). Hsp70 and Hsp40 alone had no effect on SEVI fibrils (Figure 1D). By contrast, the ThT fluorescence intensity of SEVI fibrils incubated with Hsp104, Hsp70, and Hsp40 decreased to ~36% of the initial value after 2 hr, and a larger reduction to ~16% was observed after 24 hr (Figure 1D). Thus, there is a slight enhancement in remodeling in the presence of Hsp70 and Hsp40, particularly after extended incubation times.

Next, we explored the effects of inactive Hsp104 variants on SEVI fibril integrity. $Hsp104^{DWB}$ is an ATPase-deficient Hsp104 variant with E285Q and E687Q substitutions at Walker B sites that are critical for ATP hydrolysis (Bosl et al., 2005). $Hsp104^{DWB}$ can bind but not hydrolyze ATP, which renders the protein inactive in amyloid remodeling and disaggregation (DeSantis et al., 2012). $Hsp104^{DWB}$ is also a "trap" mutant, which binds to substrates without releasing them (Bosl et al., 2005). SEVI fibrils incubated with $Hsp104^{DWB}$ for 24 hr exhibited no change in ThT fluorescence (Figure 1A). $Hsp104^{DWB}$ had no effect on fibril integrity (Figure 1E). Thus, Hsp104 actively remodels SEVI fibrils through cycles of ATP binding and hydrolysis and not merely through passive binding events.

Next, we tested the efficacy of ClpB, the *Escherichia coli* homolog of Hsp104, which can renature and remodel disordered aggregates but has limited ability to disassemble amyloid fibrils due to altered inter-subunit collaboration (DeSantis et al., 2012). ClpB did not reduce ThT fluorescence intensity when incubated with SEVI fibrils (Figure 1A). TEM confirmed that intact SEVI amyloid fibrils persisted after incubation with ClpB (Figure 1E). Thus, ClpB is unable to remodel SEVI fibrils.

To determine whether Hsp104 dissolved SEVI fibrils, we passaged reactions through a 10-kDa molecular weight cutoff filter. The resulting filtrate and retentate were analyzed by SDS-PAGE. Because the PAP248-286 peptide is ~4.5 kDa, only PAP248-286 monomers and dimers pass through the filter while any higher-order species are retained. At all time points, Hsp104-remodeled SEVI products were predominately retained by the filter (Figure 1F). Thus, dissolution of SEVI fibrils into PAP248-286 monomers or dimers by Hsp104 is not a major pathway. Rather, as suggested by TEM (Figure 1B), the products are likely larger non-fibrillar aggregates. Thus, Hsp104 has limited ability to dissolve SEVI fibrils, unlike several other amyloids (DeSantis et al., 2012). Hsp104 has reduced ability to dissolve specific Sup35 prion strains, but instead converts them to a mixture of soluble protein and non-templating aggregated forms (DeSantis and Shorter, 2012b; Shorter and Lindquist, 2006). Hsp104 transforms SEVI fibrils into another aggregated form, which likely lacks cross-β structure as indicated by reduced ThT fluorescence (Figure 1A), but can these aggregated species template the assembly of SEVI fibrils?

To assess whether Hsp104 eliminated the self-templating activity of SEVI fibrils, we tested the ability of Hsp104-remodeled SEVI products to seed fibrillization of PAP248-286. Assembly of PAP248-286 into SEVI fibrils is accelerated by addition of a small amount of preformed SEVI fibril seed, which eliminates the lag phase for nucleation (Ye et al., 2009). In the presence of 0.1% SEVI fibril seed, the lag phase for assembly was abolished, and monomeric PAP248-286 polymerized into fibrils, with ThT fluorescence intensity plateauing around 24 hr (Figure 1G). At this time, unseeded reactions remained in lag phase (Figure 1G). Importantly, SEVI fibrils pretreated with Hsp104 for 6 hr no longer seeded fibrillization of PAP248-286 (Figure 1G). Thus, Hsp104 converts SEVI fibrils into altered non-amyloid conformers that lack seeding activity.

A Potentiated Hsp104 Variant Remodels SEVI at Nanomolar Concentrations

Next, we assessed whether a potentiated Hsp104 variant had improved ability to remodel SEVI fibrils. A missense mutation in the coiled-coil middle domain of Hsp104, $Hsp104^{A503V}$, yields a potentiated variant with elevated ATPase activity, accelerated substrate translocation rate, and enhanced disaggregase activity (Jackrel et al., 2014). $Hsp104^{A503V}$ suppresses TDP-43 and α-synuclein proteotoxicity by dissolution of protein aggregates and restoration of proper protein localization (Jackrel et al., 2014; Jackrel and Shorter, 2014; Sweeny et al., 2015).

When tested against SEVI fibrils, $Hsp104^{A503V}$ reduced ThT fluorescence by a magnitude similar to that observed with Hsp104 (Figures 1A and 2A). After 2 hr with $Hsp104^{A503V}$, ThT

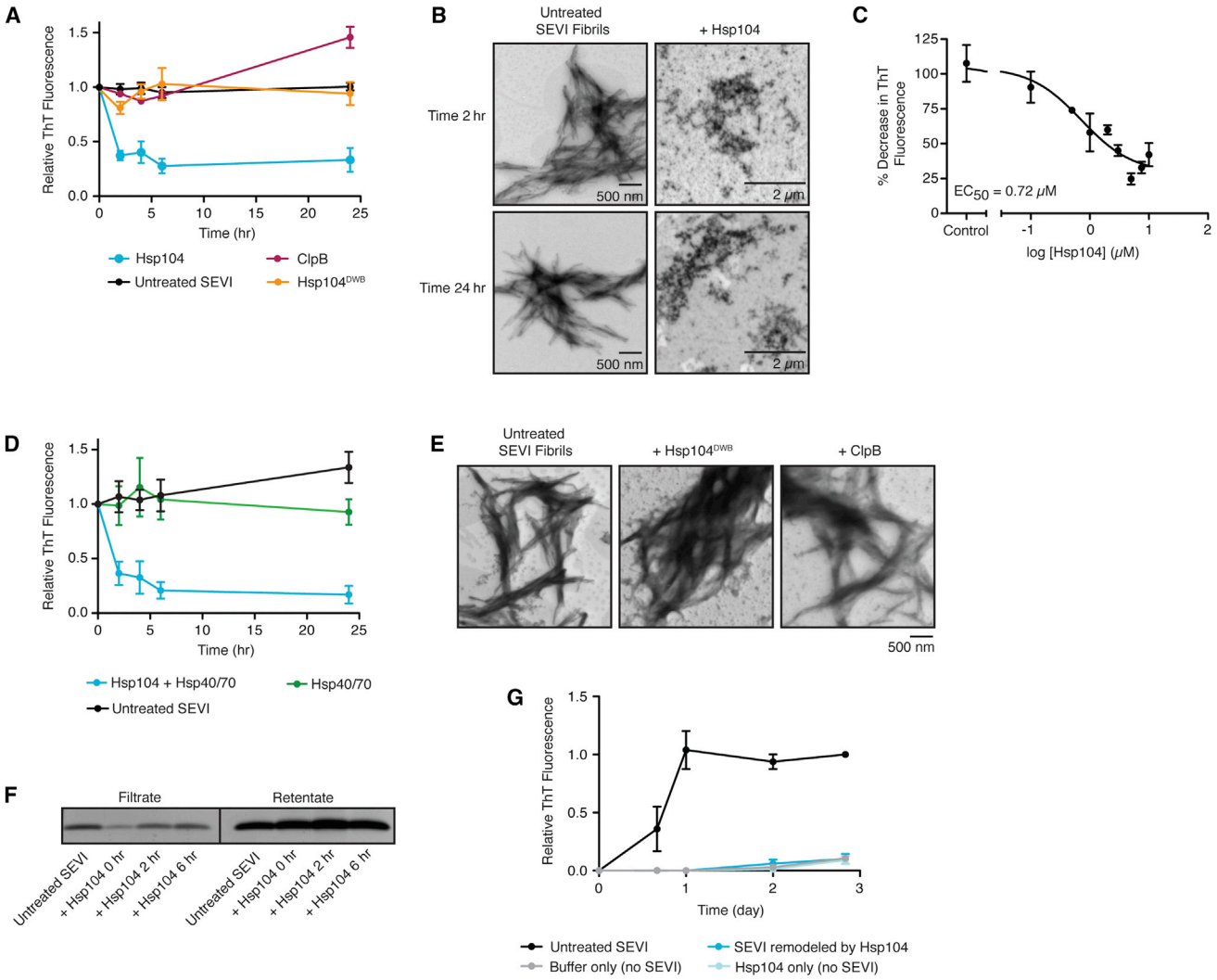

Figure 1. Hsp104 Rapidly Remodels SEVI Fibrils to Non-templating Forms

(A) SEVI fibrils (20 μM monomer) were incubated with buffer (untreated), Hsp104 (3 μM), Hsp104^{DWB} (3 μM), or ClpB (3 μM; DnaK (3 μM), DnaJ (0.6 μM), and GrpE (0.3 μM)) for 0–24 hr. Fibril integrity was assessed via ThT fluorescence. Values represent means ± SEM (n = 3–4).

(B) TEM of SEVI fibrils incubated with buffer (untreated) or Hsp104 (3 μM) for either 2 or 24 hr. Scale bars are indicated.

(C) Dose-response analysis of SEVI fibrils (20 μM monomer) treated with various concentrations of Hsp104 for 6 hr. Fibril integrity was assessed via ThT fluorescence and the EC_{50} was calculated. Values represent means ± SEM (n = 3).

(D) SEVI fibrils (20 μM monomer) were incubated with buffer (untreated) or the indicated combinations of Hsp104 (3 μM), Hsp70 (1 μM) and Hsp40 (1 μM). Fibril integrity was assessed via ThT fluorescence. Values represent means ± SEM (n = 4).

(E) TEM of SEVI fibrils incubated with buffer (untreated), Hsp104^{DWB}, or ClpB (3 μM) for 3 hr. Scale bar is indicated.

(F) SEVI fibrils (20 μM monomer) were incubated with buffer (untreated) or Hsp104 (3 μM) for 0–6 hr. The resulting products were passed over a 10 kDa filter. Filtrate and retentate fractions were processed for SDS-PAGE and silver stain.

(G) SEVI fibrils (20 μM monomer) were incubated with buffer (untreated) or Hsp104 (3 μM) for 6 hr, and the resulting products were used to seed soluble PAP248-286 (1 mM, 0.1% fibril seed) fibrillization. Buffer conditions lacking fibril seed were included. Fibril assembly was monitored by ThT fluorescence. Values represent means ± SEM (n = 4).

See also Figures S1 and S2.

fluorescence decreased to ~49% of the initial value, with a further decrease to ~35% after 24 hr (Figure 2A). Non-fibrillar aggregates accumulated after Hsp104^{A503V} treatment comparable with those observed with Hsp104 (Figure 2B). Indeed, Hsp104^{A503V} did not dissolve SEVI fibrils (Figure 2C). These aggregates were stable over several days and were unable to seed assembly of soluble PAP248-286 (Figure 2D). Thus, Hsp104^{A503V} converts SEVI fibrils to non-templating species. Remarkably, dose-response studies of Hsp104^{A503V}-catalyzed remodeling of SEVI fibrils established an EC_{50} of ~36 nM (Figure 2E), which is ~20-fold lower than the EC_{50} determined for Hsp104 (Figure 1C). This nanomolar EC_{50} for SEVI remodeling by Hsp104^{A503V} is unprecedented and could have therapeutic potential.

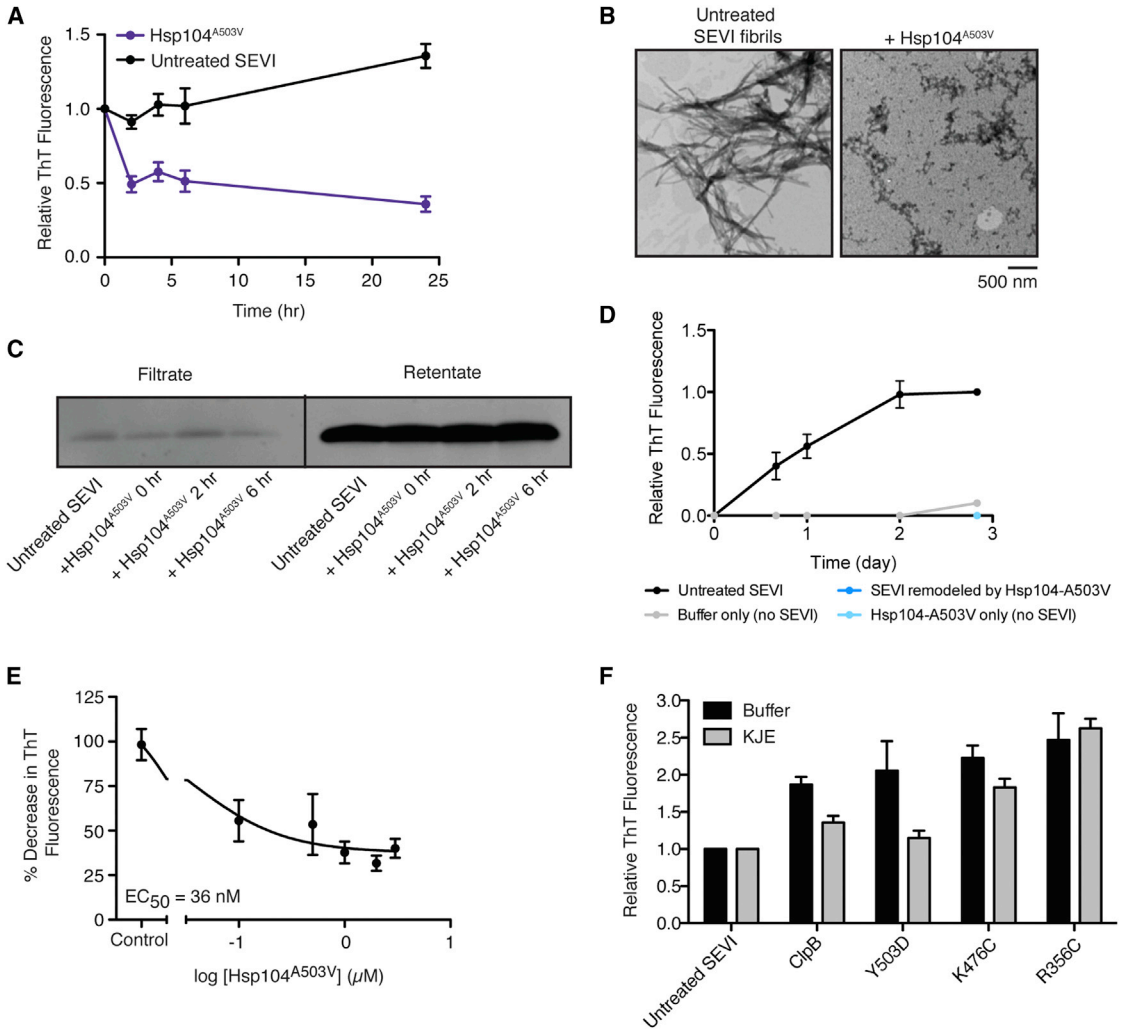

Figure 2. Hsp104^{A503V} Rapidly Remodels SEVI Fibrils, whereas Hyperactive ClpB Variants Are Inactive

(A) SEVI fibrils (20 μM monomer) were incubated with buffer (untreated) or Hsp104^{A503V} (3 μM) for 0–24 hr and fibril integrity was assessed by ThT fluorescence. Values represent means ± SEM (n = 4).

(B) TEM of SEVI fibrils incubated with buffer (untreated) or Hsp104^{A503V} (3 μM) for 3 hr. Scale bar is indicated.

(C) SEVI fibrils (20 μM monomer) were incubated with Hsp104^{A503V} (3 μM) for 0–6 hr, and the resulting products were passed over a 10-kDa filter. Filtrate and retentate fractions were then processed for SDS-PAGE and silver stain.

(D) SEVI fibrils (20 μM monomer) were incubated with buffer (untreated) or Hsp104^{A503V} (3 μM) for 6 hr, and the resulting products were used to seed soluble PAP248-286 (1 mM, 0.1% fibril seed) fibrillization. Buffer conditions lacking fibril seed were included. Fibril assembly was monitored by ThT fluorescence. Values represent means ± SEM (n = 3).

(E) Dose-response analysis of Hsp104^{A503V} remodeling of SEVI fibrils (20 μM monomer) after 6 hr of treatment. The EC_{50} is based on ThT fluorescence. Values represent means ± SEM (n = 6).

(F) SEVI fibrils (20 μM monomer) were incubated with buffer (untreated) or the indicated ClpB variant (3 μM) in the absence (black bars) or presence (gray bars) of DnaK (3 μM), DnaJ (0.6 μM), and GrpE (0.3 μM) for 6 hr, and fibril integrity was assessed by ThT fluorescence. Values represent means ± SEM (n = 3–4). See also Figures S1 and S2.

Hyperactive ClpB Variants Are Unable to Eliminate SEVI Fibrils

Next, we assessed whether ClpB activity might also be enhanced against SEVI fibrils by specific middle-domain mutations that enhance ClpB activity. Thus, we assessed the activity of three hyperactive ClpB variants: ClpB^{R356C}, ClpB^{K476C}, and ClpB^{Y503D} (Oguchi et al., 2012). None of the hyperactive ClpB variants reduced ThT fluorescence of SEVI fibrils in the presence or absence of the *E. coli* Hsp70 chaperone system: DnaK, DnaJ, and GrpE (Figure 2F). In fact, in the absence of DnaK, DnaJ, and GrpE, ClpB and the hyperactive variants increased ThT fluorescence of SEVI fibrils (Figure 2F), which might indicate a ClpB activity that exposes further ThT-binding sites on SEVI fibrils. DnaK, DnaJ, and GrpE had no effect on SEVI fibrils alone and prevented the increase in ThT fluorescence caused by ClpB or ClpB^{Y503D}, but not ClpB^{R356C} or ClpB^{K476C} (Figure 2F). Thus, ClpB is unable to eliminate amyloid even when its activity is enhanced by hyperactivating mutations in the middle domain. This finding likely

reflects profound differences in how Hsp104 and ClpB subunits process substrates for disaggregation (DeSantis et al., 2012, 2014).

Hsp104 and Hsp104^{A503V} Remodel PAP85-120 Fibrils

The relative contribution of each seminal amyloid to enhancement of HIV infection by human semen is uncertain and thus it is important to isolate amyloid-remodeling factors that remodel diverse seminal amyloids (Castellano and Shorter, 2012). We examined whether Hsp104 and Hsp104^{A503V} remodel additional amyloid fibrils endogenous to seminal fluid, including those formed by another PAP fragment, PAP85-120 (Arnold et al., 2012). Hsp104 remodeled PAP85-120 fibrils, whereas ClpB and Hsp104^{DWB} were inactive (Figure S1A). After 2 hr, Hsp104 reduced ThT fluorescence to ~63% of the initial value, and a further decrease to ~39% was observed after 6 hr, indicating rapid fibril remodeling (Figure S1A). Hsp104 remodels PAP85-120 fibrils into non-fibrillar aggregates (Figure S1B). Similar results were obtained with Hsp104^{A503V} (Figures S1C and S1D). Under these conditions, the ThT fluorescence intensity decreased more slowly than with Hsp104, and a reduction to only ~67% was observed after 2 hr (Figure S1C). However, after 24 hr of incubation with Hsp104^{A503V}, ThT fluorescence decreased to ~28% of the initial value (Figure S1C). TEM analysis also revealed non-amyloid aggregates after treatment with Hsp104^{A503V} (Figure S1D). Thus, Hsp104 and Hsp104^{A503V} rapidly remodel SEVI and PAP85-120 fibrils.

Hsp104 and Hsp104^{A503V} Do Not Remodel SEM1(45–107) Fibrils

Numerous peptide fragments of SEM1 and SEM2 form amyloid and enhance HIV infection (Roan et al., 2011). We focused on the SEM1(45–107) fragment as a representative peptide. ThT fluorescence was unchanged when SEM1(45–107) fibrils were treated with Hsp104 or Hsp104^{A503V} for 24 hr (Figures S2A and S2C). This result was verified by TEM, which showed abundant, dense clumps of SEM1(45–107) fibrils after Hsp104 or Hsp104^{A503V} treatment (Figures S2B and S2D). Thus, SEM1(45–107) fibrils are refractory to remodeling by Hsp104 and Hsp104^{A503V}, indicating that some feature of SEM1(45–107) fibrils antagonizes Hsp104 activity.

Hsp104 Promotes Clustering of Seminal Amyloid into Larger Aggregates

Even though Hsp104^{DWB} and ClpB failed to eliminate cross-β structure of seminal amyloid as indicated by ThT fluorescence (Figures 1A, S1A, and S2A), solutions became turbid, indicating a clustering of fibrils into higher-order conglomerates. Sequestration of seminal amyloid into larger aggregated structures could be a valuable strategy, as it would shield the network of positive charge presented by fibrils and reduce stimulation of HIV infection. Indeed, molecular chaperones stimulate clustering of toxic misfolded oligomers into larger species in the absence of any structural reorganization or disassembly of oligomers (Mannini et al., 2012). The larger aggregated species mask reactive surfaces of oligomers and neutralize oligomer toxicity (Mannini et al., 2012). Importantly, this mechanism is extremely effective, as significant effects are observed at highly substoichiometric chaperone levels (Mannini et al., 2012). Moreover, several chaperones do not require ATP or ATPase activity to cluster oligomers (Mannini et al., 2012). By analogy, we wondered whether Hsp104-based scaffolds might cluster seminal amyloid into larger aggregates in an ATP-independent manner and neutralize their ability to promote HIV infection.

We employed turbidity to assess the formation of larger aggregates. GFP was included as a protein control and did not affect turbidity of any of the seminal amyloid fibrils (Figures 3A–3C). By contrast, the turbidity of SEVI, PAP85-120, and SEM1(45–107) fibrils increased rapidly upon incubation with Hsp104, Hsp104^{DWB}, or ClpB (Figures 3A–3C and S3A–S3C). Thus, Hsp104 remodels the amyloid structure of SEVI and PAP85-120 fibrils (Figures 1A and S1A) and simultaneously transforms these conformers into large amorphous aggregates (Figures 1B, 3A, 3B, and S1B). By contrast, Hsp104 does not remodel SEM1(45–107) fibrils but clusters them into large aggregates (Figures S2A and 3C). Hsp104^{DWB} and ClpB fail to remodel the amyloid structure of SEVI, PAP85-120, and SEM1(45–107) fibrils (Figures 1A, S1A, and S2A), but cluster them into larger species (Figures 3A–3C and S3A–S3C). A marginally larger increase in turbidity was observed when seminal amyloid fibrils were incubated with Hsp104^{DWB} in comparison with Hsp104 (Figures 3A–3C). Thus, the seminal amyloid clustering activity does not require ATP hydrolysis and resembles clustering of toxic oligomers into larger aggregates by various chaperones (Mannini et al., 2012).

To confirm this clustering effect, dynamic light scattering (DLS) was used to investigate the size distribution profile of seminal amyloid in the absence and presence of Hsp104, Hsp104^{DWB}, or GFP. DLS of Hsp104 alone revealed species with a diffusion coefficient of ~2.7 × 10^{-7} cm^2/s and hydrodynamic radius (R_h) of ~7–10 nm (Figure S4A), indicative of a hexamer and consistent with prior studies (Bosl et al., 2005; Narayanan et al., 2003; Sweeny et al., 2015). Soluble PAP248-286 peptide had an R_h of ~1–2 nm (Figure S4B), which might indicate dimeric forms or an extended, unstructured monomer (Brender et al., 2011). By contrast, untreated SEVI fibrils contained an assortment of species with different R_h values (Figure 3D). The major species had R_h of ~6 nm and ~1,000–3,000 nm (Figure 3D). The DLS profile shifted drastically upon addition of Hsp104 or Hsp104^{DWB}, revealing a broad size distribution of larger particles ranging in R_h of ~100–10,000 nm (Figures 3E and 3F). In contrast, when SEVI fibrils were incubated with GFP, the size distribution profile closely resembled the buffer control (Figures 3D and 3G). Similarly, in the presence of Hsp104 and Hsp104^{DWB}, the size distribution profile of SEM1(45–107) fibrils shifted toward larger species (Figures 3H–3J). Indeed, aggregated species were now observed with R_h >5,000 nm (Figures 3I and 3J), which are not observed in the buffer control (Figure 3H). Contrastingly, the particle sizes of SEM1(45–107) fibrils treated with GFP were more similar to the buffer control (Figures 3H and 3K). These data suggest that Hsp104 and Hsp104^{DWB} cluster PAP248-286 and SEM1(45–107) into larger aggregated species.

Next, we tested whether Hsp104 hexamers or ATP were required for clustering activity. Thus, we explored three monomeric Hsp104 fragments: Hsp104$^{1-548}$, comprising the N-terminal domain (NTD), nucleotide-binding domain 1 (NBD1), and middle domain of Hsp104; Hsp104$^{773-908}$, comprising the

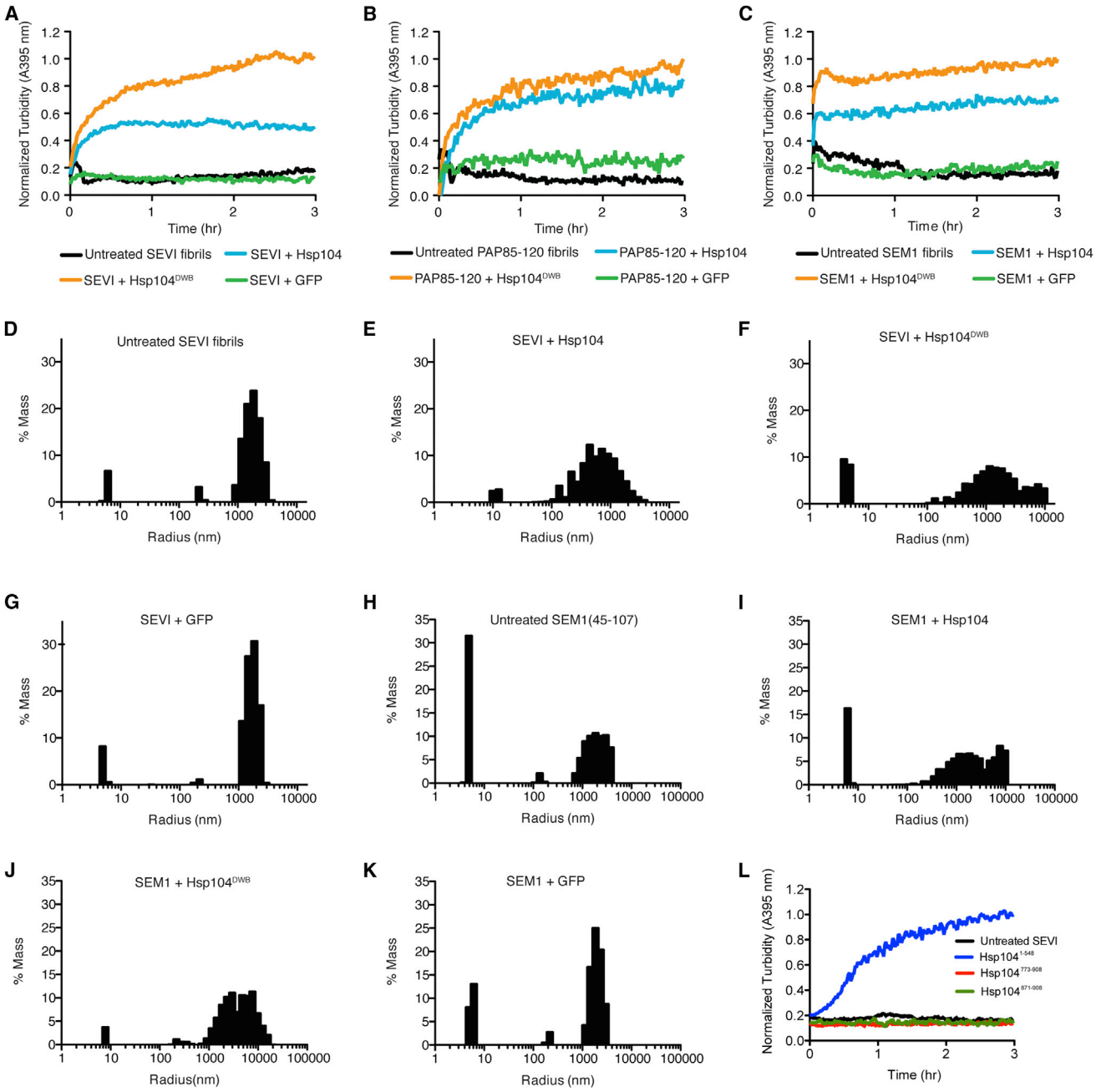

Figure 3. Hsp104 Promotes the Clustering of Seminal Amyloid Fibrils into Larger Aggregates

(A–C) SEVI (A), PAP85-120 (B), and SEM1(45–107) (C) fibrils (20 μM monomer) were incubated with Hsp104, Hsp104^{DWB}, ClpB, or GFP (1.8 μM monomer), and absorbance at 395 nm was measured for 3 hr. One representative trial is shown.

(D–G) DLS was used to determine the size distribution by mass of SEVI fibrils (20 μM monomer) treated with buffer (D), Hsp104 (E), Hsp104^{DWB} (F), or GFP (G) (1.8 μM monomer) for ~5 min at 25°C.

(H–K) DLS was used to determine the size distribution by mass of SEM1(45–107) fibrils (20 μM monomer) treated with buffer (H), Hsp104 (I), Hsp104^{DWB} (J), or GFP (K) (1.8 μM monomer) for ~5 min at 25°C.

(L) SEVI fibrils (20 μM) were incubated with Hsp104$^{1-548}$, Hsp104$^{773-908}$, or Hsp104$^{871-908}$ (1.8 μM monomer), and absorbance at 395 nm was measured for 3 hr. One representative trial is shown. See also Figures S3 and S4.

small domain of NBD2 and the C-terminal domain of Hsp104, which can engage basic substrates such as polylysine; and Hsp104$^{871-908}$, comprising the C-terminal acidic tail of Hsp104 (Cashikar et al., 2002; Hattendorf, 2001). Remarkably, incubation of SEVI, PAP85-120, and SEM1(45–107) fibrils with Hsp104$^{1-548}$, but not Hsp104$^{773-908}$ or Hsp104$^{871-908}$, resulted in a substantial increase in turbidity (Figures 3L, S3D, and S3E). Importantly, Hsp104$^{1-548}$, Hsp104$^{773-908}$, and Hsp104$^{871-908}$ were unable

to remodel SEVI or PAP85 fibrils as indicated by ThT fluorescence (data not shown). Thus, neither Hsp104 hexamerization nor ATP hydrolysis is necessary for clustering activity. Rather, determinants in the first 548 amino acids of Hsp104 are sufficient to promote clustering, whereas the C-terminal 136 amino acids are unable to promote clustering. Importantly, the inability of the acidic C-terminal tail of Hsp104 (p*I* = 3.28), Hsp104$^{871-908}$, to promote clustering suggests that simply being negatively charged is not sufficient to induce clustering. Clustering of seminal amyloid into larger conglomerates likely decreases availability of virion-binding sites on fibrils via occlusion.

HAP Plus ClpP Degrades SEVI Fibrils and PAP85-120 Fibrils

A potential problem with the seminal amyloid-remodeling activity of Hsp104 (Figures 1, 2, and S1) is that peptides might eventually reform amyloid and promote HIV infection. Likewise, the clustering of seminal amyloid into larger aggregates by various Hsp104 scaffolds (Figure 3) might also be reversed and enable fibrils to promote HIV infection. To irrevocably remove seminal amyloid, we coupled Hsp104 remodeling activity to proteolysis. For this we employed HAP, an Hsp104 variant carrying three missense mutations (G739I:S740G:K741F) in a helix-loop-helix motif that enables association with ClpP, a chambered peptidase from *E. coli* akin to the proteasome (Tessarz et al., 2008). HAP maintains disaggregase activity and substrate recognition, but threads disaggregated products through its central pore and into the proteolytic chamber of ClpP for degradation (Tessarz et al., 2008).

Like Hsp104 (Figure 1A), HAP or HAP plus ClpP effectively remodeled SEVI fibrils, whereas ClpP alone was ineffective (Figure 4A). After 24 hr, HAP or HAP plus ClpP reduced ThT fluorescence to ~22% (Figure 4A). Importantly, this decrease in ThT fluorescence occurred when SEVI fibrils were subjected to substoichiometric concentrations of HAP or HAP plus ClpP. In fact, the EC_{50} for SEVI fibril remodeling by HAP was ~0.36 μM (Figure 4B), and a slighter higher EC_{50} of ~1.28 μM was determined for HAP plus ClpP (Figure 4C), indicating that ClpP reduces HAP efficacy (Shorter and Lindquist, 2005).

TEM revealed that HAP or HAP plus ClpP converted SEVI fibrils to amorphous aggregates, similar to those observed with Hsp104, whereas ClpP alone was ineffective (Figures 1B and 4D). The extreme stability of the amyloid fold resists disruption by proteases and protein denaturants (Vashist et al., 2010). Thus, as expected, ClpP alone was unable to degrade SEVI fibrils (Figure 4E), although it was able to rapidly degrade soluble PAP248-286 in the presence or absence of HAP (Figure 4E). Usually ClpP alone cannot degrade folded proteins without a cognate AAA+ ATPase partner (Yu and Houry, 2007). Indeed, only small peptides typically shorter than six residues are able to enter the ClpP chamber for degradation (Wang et al., 1997). Thus, soluble PAP248-286 is likely to be unfolded and must effectively access the proteolytic chamber of ClpP. Importantly, HAP plus ClpP degraded SEVI fibrils over the course of 24 hr (Figure 4E). Accordingly, HAP plus ClpP eliminated the ability of SEVI fibrils to seed fibrillization of soluble PAP248-286, confirming a deconstruction of amyloid structure (Figure 4F). To the best of our knowledge, this is the first example of a proteolytic system that can effectively remodel and degrade amyloid.

HAP plus ClpP also rapidly degraded the soluble SEM1(45–107) and PAP85-120 peptides, whereas ClpP alone was ineffective (Figures 4G and 4H). HAP plus ClpP was unable to degrade SEM1(45–107) fibrils (Figure 4G), which is consistent with the inability of Hsp104 to remodel SEM1(45–107) fibrils (Figure S2A). By contrast, HAP plus ClpP degraded PAP85-120 fibrils, whereas ClpP alone was ineffective (Figure 4H). Thus, HAP plus ClpP degrades SEVI and PAP85-120 fibrils.

Fibril Remodeling, Clustering, and Degradation Reduce Stimulation of HIV Infection

Finally, we assessed whether these Hsp104-based treatments affected the ability of seminal amyloids to promote HIV infection. We employed TZM-bl cells containing a luciferase reporter construct under control of the HIV-1 long terminal repeat to assess the extent of infectivity. First, we determined that Hsp104, Hsp104^{A503V}, Hsp104^{DWB}, ClpB, Hsp104$^{1-548}$, Hsp104$^{773-908}$, HAP, ClpP, and GFP had no effect on HIV infection of TZM-bl cells in the absence of seminal amyloid (Figure 5A). Moreover, none of the Hsp104 conditions affected cell viability (Figure 5B; data not shown). Thus, any effects of Hsp104-based treatments were due to an effect on the fibrils rather than any direct effect on HIV or on cell viability.

Hsp104 and variants were unable to remodel or degrade SEM1(45–107) fibrils (Figure S2A, S2C, and 4G), but Hsp104, Hsp104^{DWB}, and ClpB clustered them into larger conglomerates, whereas GFP was ineffective (Figures 3C and S3C). Remarkably, this clustering activity reduced the ability of SEM1(45–107) fibrils to promote HIV infection, whereas GFP and ClpP were ineffective (Figure 5C). Hsp104^{DWB} converted SEM1(45–107) fibrils into the largest structures (Figures 3C and 3J) and accordingly caused the largest reduction in HIV infection (Figure 5C). The partitioning of SEM1(45–107) amyloid into larger aggregates likely decreases the availability of virion-binding sites and thereby restricts the enhancement of infection (Figure 6). Thus, seminal amyloid fibrils must be disseminated to counter electrostatic repulsion and promote HIV infection (Figure 6). Clustering seminal amyloid into large conglomerates reduces their ability to enhance HIV infection.

Hsp104-based treatments that remodeled, clustered, or degraded SEVI fibrils or PAP85-120 fibrils reduced their ability to promote HIV infection (Figures 5D–5F and 6). Thus, Hsp104$^{773-908}$, ClpP, and GFP, which could neither remodel, cluster, nor degrade SEVI fibrils or PAP85-120 fibrils, had no effect on their ability to enhance HIV infection (Figures 5D and 5E). Hsp104$^{871-908}$ also had no effect on the ability of SEVI fibrils to enhance HIV infection (Figure S5). By contrast, Hsp104, Hsp104^{A503V}, or HAP remodeled SEVI fibrils (Figures 1A, 2A, and 4A) and PAP85-120 fibrils (Figure S1A), and reduced their ability to enhance HIV infection (Figures 5D–5F). Hsp104^{DWB}, ClpB, and Hsp104$^{1-548}$, which clustered SEVI fibrils or PAP85-120 fibrils, also reduced enhancement of HIV infection (Figures 5D–5F). Finally, HAP plus ClpP degraded SEVI and PAP85-120 fibrils (Figures 4E and 4H) and strongly reduced enhancement of HIV infection (Figures 5D and 5E). Thus, fibril remodeling, clustering, and degradation can all reduce the enhancement of HIV infection by seminal amyloid (Figures 6C and 6D).

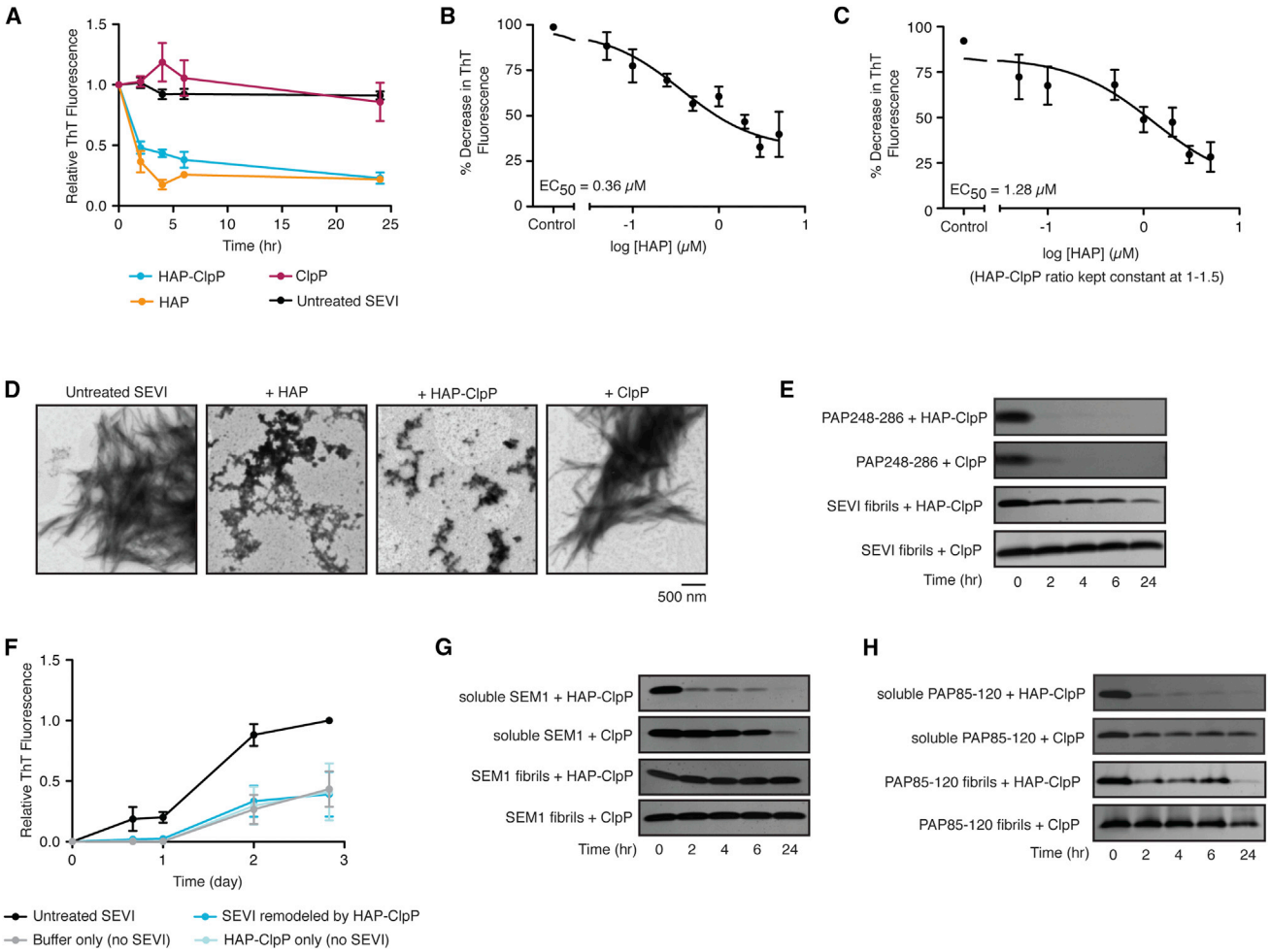

Figure 4. HAP Plus ClpP Degrades SEVI Fibrils and PAP85-120 Fibrils

(A) SEVI fibrils (20 μM monomer) were incubated with buffer (untreated), HAP (3 μM), ClpP (4.5 μM), or HAP (3 μM) plus ClpP (4.5 μM) for 0–24 hr. Fibril integrity was assessed via ThT fluorescence. Values represent means ± SEM (n = 3–4).

(B and C) Dose-response analysis for HAP (B) and HAP plus ClpP (C) remodeling of SEVI fibrils (20 μM monomer) after 6 hr. The EC_{50} is based on ThT fluorescence. Values represent means ± SEM (n = 3–7).

(D) TEM of SEVI fibrils (20 μM monomer) incubated with buffer (untreated), HAP (3 μM), ClpP (4.5 μM), or HAP (3 μM) plus ClpP (4.5 μM) for 24 hr. Scale bar is indicated.

(E) SEVI fibrils or soluble PAP248-286 (20 μM monomer) were treated with HAP (3 μM), ClpP (4.5 μM), or HAP (3 μM) plus ClpP (4.5 μM) for 0–24 hr at 37°C. Reactions were then processed for SDS-PAGE and silver stain.

(F) SEVI fibrils (20 μM monomer) were incubated with HAP (3 μM) and ClpP (4.5 μM) for 6 hr, and the resulting products were used to seed soluble PAP248-286 (1 mM, 0.1% fibril seed) fibrillization. Buffer conditions lacking fibril seed were included. Fibril assembly was monitored by ThT fluorescence. Values represent means ± SEM (n = 4).

(G and H) PAP85-120 fibrils or soluble PAP85-120 (G) or SEM1(45–107 fibrils) or SEM1(45–107) (20 μM monomer) (H) were treated with HAP (3 μM), ClpP (4.5 μM), or HAP (3 μM) plus ClpP (4.5 μM) for 0–24 hr at 37°C, then processed for SDS-PAGE and silver stain.

DISCUSSION

We have repurposed an amyloid-remodeling nanomachine from yeast, Hsp104, to antagonize seminal amyloid and reduce amyloid-mediated enhancement of HIV infection. Hsp104, as well as $Hsp104^{A503V}$, a potentiated Hsp104 variant (Jackrel and Shorter, 2015), were highly effective at rapidly remodeling SEVI and PAP85-120 fibrils into non-fibrillar structures. In contrast to a variety of other amyloids (DeSantis et al., 2012), the major Hsp104-catalyzed remodeling pathway was not the conversion of SEVI or PAP85-120 fibrils to soluble peptide, but rather the conversion of fibrils to an alternative aggregated state. This remodeling activity required ATP hydrolysis, as $Hsp104^{DWB}$ was ineffective. The *E. coli* Hsp104 homolog, ClpB, was unable to remodel SEVI or PAP85-120 fibrils, even when activated by mutations in the middle domain that enhance activity (Oguchi et al., 2012). The inability of even hyperactive ClpB variants to remodel amyloid likely reflects profound differences in how Hsp104 and ClpB subunits process substrates for disaggregation (DeSantis et al., 2012). In stark contrast, $Hsp104^{A503V}$ remodeled SEVI fibrils (20 μM monomer) at extremely low concentrations, with a calculated EC_{50} value in the nanomolar range. An EC_{50} this low relative

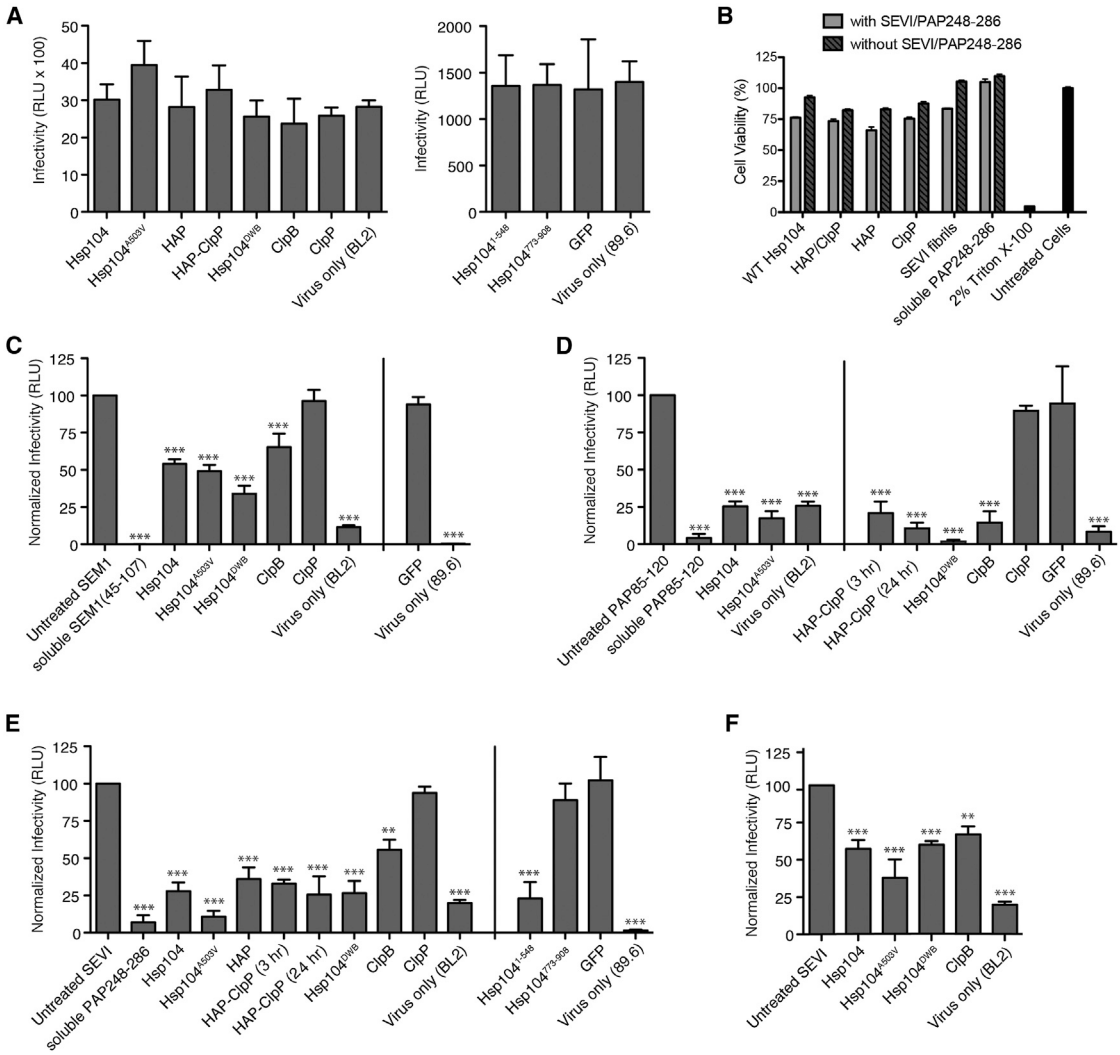

Figure 5. Hsp104 Reduces the Ability of Seminal Amyloid to Enhance HIV Infection

(A) Effect of Hsp104 variants and ClpP on viral infectivity (left: BL2 virions; right: 89.6 virions) in the absence of any enhancing seminal amyloid. Values represent means ± SEM (n = 3–6).

(B) MTT assay reveals that the various conditions do not affect TZM-bl cell viability, unlike the TX-100 control. Values represent means ± SEM (n = 3–5).

(C) SEM1(45–107) fibrils (20 μM monomer) were pretreated with buffer, Hsp104, Hsp104^{A503V}, Hsp104^{DWB}, ClpB, ClpP, or GFP, and HIV infectivity was assessed in TZM-bl cells by measuring luciferase activity (in relative light units). Different viral strains were used for samples on either side of the solid line. Values represent means ± SEM (n = 3–6). A one-way ANOVA with the post hoc Dunnett's multiple comparisons test was used to compare the untreated SEM1 control with all other conditions (***$p < 0.001$).

(D) PAP85-120 fibrils (20 μM) were pretreated with buffer, Hsp104, Hsp104^{A503V}, Hsp104^{DWB}, ClpB, ClpP, HAP plus ClpP, or GFP, and HIV infectivity was assessed in TZM-bl cells and expressed as normalized infectivity to untreated fibril samples. Different viral strains were used for samples on either side of the solid line. Values represent means ± SEM (n = 3–4). A one-way ANOVA with the post hoc Dunnett's multiple comparisons test was used to compare the untreated PAP85-120 control with all other conditions (***$p < 0.001$).

(E) SEVI fibrils (20 μM) were pretreated with buffer, Hsp104, Hsp104^{A503V}, Hsp104^{DWB}, ClpB, Hsp104$^{1-548}$, Hsp104$^{773-908}$, HAP, ClpP, HAP plus ClpP, or GFP, and HIV infectivity was assessed in TZM-bl cells and expressed as normalized infectivity to untreated fibril samples. Different viral strains were used for samples on either side of the solid line. Values represent means ± SEM (n = 3–7). For all experiments in (A) to (E), the protein concentrations used were: Hsp104 (3 μM), Hsp104^{A503V} (3 μM), HAP (3 μM), HAP-ClpP (3 μM and 4.5 μM, respectively), Hsp104^{DWB} (3 μM), Hsp104$^{1-548}$ (18 μM monomer), Hsp104$^{773-908}$ (18 μM monomer), ClpB (3 μM), ClpP (18 μM monomer), and GFP (18 μM monomer). A one-way ANOVA with the post hoc Dunnett's multiple comparisons test was used to compare the untreated SEVI control with all other conditions (***$p < 0.001$; **$p < 0.01$).

(F) SEVI fibrils were treated as in (E) except that the Hsp104 variant concentration was 0.3 μM. HIV infectivity was assessed in TZM-bl cells and expressed as normalized infectivity to untreated fibril samples. Values represent means ± SEM (n = 3–7). A one-way ANOVA with the post hoc Dunnett's multiple comparisons test was used to compare the untreated SEVI control with all other conditions (***$p < 0.001$; **$p < 0.01$).

See also Figure S5.

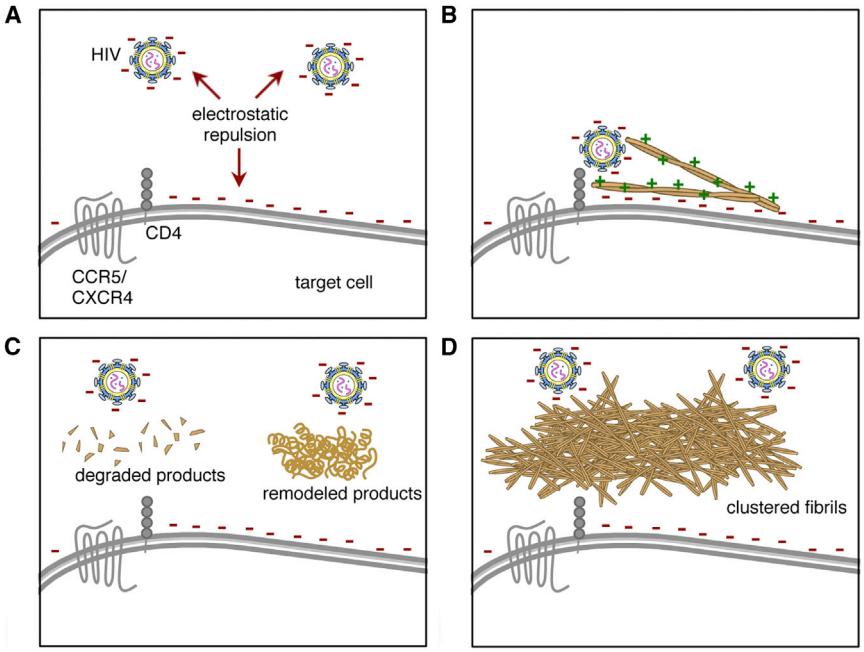

Figure 6. Hsp104-Based Treatments that Remodel, Degrade, or Cluster Seminal Amyloid Reduce their Ability to Stimulate HIV Infection

(A) In the absence of seminal amyloid, HIV infectivity is limited by electrostatic repulsion between the negatively charged surfaces of the viral and target cell membranes.

(B) Cationic seminal amyloid fibrils shield this electrostatic repulsion and facilitate HIV infectivity by bringing virions in closer proximity to the cell surface.

(C) Hsp104-based treatments remodel (Hsp104 and $Hsp104^{A503V}$) and degrade (HAP plus ClpP) SEVI and PAP85-120 fibrils such that their ability to boost infection is reduced.

(D) Hsp104-based treatments non-catalytically promote the assembly of seminal amyloid into higher-order conglomerates, which results in fewer available sites within fibrils for virion binding and also acts as a physical barrier to cell entry.

to the quantity of fibrils has not been observed for Hsp104 with any amyloid, including its natural amyloid substrate, Sup35 prions, where the EC_{50} (calculated from assays with lower quantities of fibrils relative to Hsp104) ranges from ~60 to 600 nM depending on the prion strain (DeSantis and Shorter, 2012b). Importantly, treatment of SEVI and PAP85-120 fibrils with Hsp104 or $Hsp104^{A503V}$ greatly reduced their ability to enhance HIV infection (Figure 6C).

Hsp104 engages substrates primarily via two highly conserved pore loops in NBD1 (256-KYKG-259) and NBD2 (661-GYVG-664), which project into the central channel of the hexamer (DeSantis and Shorter, 2012a). The NTD of Hsp104 also contains conserved acidic residues (D108 and D114) that bind substrate (our unpublished observations) (Barnett et al., 2005). We have shown previously that Hsp104 directly engages a range of cross-β conformers formed by diverse polypeptides (DeSantis et al., 2012). Interestingly, peptide arrays have revealed that Hsp104 displays some amino acid preferences in the context of linear peptides (Lum et al., 2008). We suspect that if preferred amino acids are presented in conformational epitopes (rather than linear motifs), Hsp104 is likely to recognize these specifically. The heightened susceptibility of SEVI and PAP85-120 fibrils to remodeling by Hsp104 and $Hsp104^{A503V}$ might reflect the high lysine content of PAP248-286 (15.4%) and PAP85-120 (8.6%) (Castellano and Shorter, 2012). Indeed, lysine-rich regions provide an important recognition feature for Hsp104, and polylysine stimulates ATP hydrolysis by Hsp104 (Cashikar et al., 2002; Lum et al., 2008). However, SEM1(45–107) contains a similar proportion of lysine residues (9.5%), and SEM1(45–107) fibrils were not remodeled by Hsp104 or $Hsp104^{A503V}$. Thus, some other feature of SEM1(45–107) fibrils likely prevents remodeling by Hsp104. One possibility is that SEM1(45–107) contains a high proportion of residues that disfavor Hsp104 binding, including serine, glycine, and histidine (Lum et al., 2008), which are less abundant in PAP248-286 and PAP85-120 (Castellano and Shorter, 2012). Thus, Hsp104 may not gain sufficient traction to remodel SEM1(45–107) fibrils. Alternatively, SEM1(45–107) fibrils might access an amyloid strain, which is intractable for other reasons such as binding-site inaccessibility or enhanced stability. A key goal is to innovate engineered Hsp104 variants that remodel SEM1(45–107) fibrils.

Remodeling amyloid structure by Hsp104 was not necessary, however, for specific Hsp104 variants to reduce the ability of seminal amyloid to enhance HIV infection. Thus, even though Hsp104 did not remodel SEM1(45–107) fibrils, it reduced their ability to enhance HIV infection. Indeed, Hsp104 clustered SEM1(45–107) fibrils into large, higher-order aggregates. This activity did not require ATP hydrolysis as $Hsp104^{DWB}$ promoted fibril clustering. Indeed, several Hsp104 variants unable to remodel amyloid structure, including ClpB, and even the monomeric Hsp104 fragment, $Hsp104^{1-548}$ encompassing the NTD, NBD1, and the middle domain, clustered seminal amyloid fibrils into larger conglomerates with reduced ability to promote HIV infection. Importantly this effect was specific, as not any protein could cluster seminal amyloid. Thus, GFP and the Hsp104 fragments, $Hsp104^{773-908}$ and $Hsp104^{871-908}$, were unable to promote seminal amyloid clustering and had no effect on the enhancement of HIV infection. The clustering of seminal amyloid into larger conglomerates likely decreases the availability of virion-binding sites on fibrils and thereby reduces the enhancement of infection (Figure 6D). Furthermore, these higher-order assemblies may act as a physical barrier, obstructing virion access to the target cell surface (Figure 6D). These findings indicate that seminal amyloid fibrils must be disseminated to counter electrostatic repulsion and promote HIV infection (Figure 6B). If fibrils become too clustered, their ability to promote HIV infection declines. Future studies will decipher the specific region within Hsp104 that is sufficient to cause seminal amyloid clustering,

which could empower the design of peptide-based inhibitors that impede seminal amyloid functionality.

The clustering activity we observed is reminiscent of the ability of various molecular chaperones to stimulate the clustering of toxic oligomers into larger species in the absence of structural reorganization of the oligomers themselves (Mannini et al., 2012). The larger aggregated species mask the reactive surfaces of oligomers and neutralize oligomer toxicity (Mannini et al., 2012). This activity does not require chaperone ATPase activity or even ATP, and can be driven by substoichiometric quantities of chaperone (Mannini et al., 2012). Hsp104 stimulates prionogenesis of various yeast prion proteins, including Sup35 and Ure2, when acting at substoichiometric concentrations (Shorter and Lindquist, 2004, 2006, 2008; Sweeny et al., 2015; Sweeny and Shorter, 2008). However, the clustering of amyloid fibrils into large conglomerates is not an activity we have observed previously with other substrates. Nonetheless, this activity, which does not require Hsp104 ATPase activity or even a hexameric structure, could play an important role in vivo in the partitioning of aggregated proteins into higher-order compartments, such as stress foci, JUNQ (juxta-nuclear quality control compartment), and IPOD (insoluble protein deposit compartment) (Amen and Kaganovich, 2015).

Therapeutically, effective Hsp104 nanomachines could be used as microbicide applied in the anogenital tract. A potential problem with remodeling seminal amyloid or clustering amyloid into higher-order structures is that remodeled peptides might reform amyloid, and clustered fibrils might disperse and be able to enhance HIV infection once again. To avoid this risk and irreversibly clear seminal amyloid, we developed a strategy that couples seminal amyloid remodeling to degradation. Thus, we engineered Hsp104 to interact with ClpP, a chambered protease from *E. coli*. The modified Hsp104 variant, termed HAP, passes remodeled substrates into the ClpP chamber for degradation (Tessarz et al., 2008). Although ineffective against SEM1(45–107) fibrils, HAP plus ClpP effectively remodeled and degraded SEVI fibrils and PAP85-120 fibrils. This ability to contemporaneously remodel and degrade exceptionally stable amyloid has not been previously reconstituted using pure components, and could also prove useful in the removal of pathologic or disease-associated amyloid fibrils. Coupled fibril remodeling and degradation could be especially advantageous in instances where reactivation of the protein sequestered in fibrils is not beneficial, as with Aβ deposits in Alzheimer's disease (Cushman et al., 2010).

SIGNIFICANCE

There is a great need for microbicidal agents that interfere with HIV infectivity without inducing tissue inflammation. Our studies suggest that seminal amyloid is likely a tractable target. We have demonstrated that various strategies based on Hsp104 interfere with the infectivity-enhancing function of seminal amyloid. The most irreversible of these entails coupled remodeling and degradation of seminal amyloid via the HAP-ClpP system. The ability to irrevocably clear seminal amyloid and block sexual transmission of HIV could provide a game-changing solution for the global HIV/AIDS pandemic. Our approach of targeting host protein conformers (seminal amyloid) is fundamentally different from traditional microbicidal approaches that target the virus. Consequently, we anticipate that this strategy will synergize with direct antiviral strategies, such that microbicides containing antiviral agents and antiamyloid agents could display enhanced efficacy.

EXPERIMENTAL PROCEDURES

Peptides and Fibril Formation

Synthetic peptide Hsp104$^{871-908}$ was from Genscript. Synthetic peptides PAP248-286, PAP85-120, and SEM1(45–107) were from the Keck Biotechnology Resource Laboratory (Yale University). Lyophilized peptides were reconstituted and assembled into fibrils as described previously (Arnold et al., 2012; Münch et al., 2007; Roan et al., 2011). In brief, lyophilized PAP248-286 was dissolved in PBS to 1 mM, passed through a 0.2-μm filter, and agitated at 37°C and 1400 rpm (Eppendorf Thermomixer) for ~72 hr. All subsequent SEVI fibrils were assembled by adding 1% fibril seed to soluble PAP248-286 solutions and agitating at 37°C and 1400 rpm overnight. Lyophilized PAP85-120 was dissolved in 1,1,1,3,3,3-hexafluoro-2-propanol (HFIP) to remove aggregates and separated into 100-μl aliquots. HFIP was removed by drying in a speed vacuum for 30 min. The resulting film was dissolved in Gibco UltraPure water to 1 mM and passed through a 0.2-μm filter, and solutions were agitated at 37°C and 1400 rpm for 24–48 hr. Lyophilized SEM1(45–107) was dissolved in PBS to 0.5 mM, passed through a 0.2-μm filter, and agitated at 37°C and 1400 rpm for 7 days. Peptide concentrations were calculated using extinction coefficients at 280 nm.

Proteins

Hsp104 and ClpB variants were generated using QuikChange mutagenesis (Agilent). Untagged Hsp104 variants (wild-type, HAP, DWB, and A503V) were overexpressed in BL21(DE3)-RIL *E. coli* cells and purified using Affi-Gel Blue (Bio-Rad) followed by Resource Q anion-exchange chromatography as described by DeSantis et al. (2014). His-tagged proteins (ClpP, ClpB, GFP, Hsp104$^{1-548}$, and Hsp104$^{773-908}$) were purified using Ni Sepharose 6 Fast Flow (GE Life Sciences) following standard procedures. His-tagged ClpP, ClpB, and Hsp104 variants were overexpressed in BL21(DE3), M15, and BL21-RIL *E. coli* cells, respectively, for purification. The reported concentrations of Hsp104 or ClpB refer to the hexamer and ClpP to the 14-mer unless otherwise indicated. Hsp70, Hsp40, DnaK, DnaJ, and GrpE were from Enzo Life Sciences.

Fibril Remodeling

For remodeling experiments, fibrils (20 μM monomer) were incubated with Hsp104, ClpB, or the indicated variant (3 μM) and diluted into an assay buffer (25 mM HEPES-KOH, 150 mM KOAc, 10 mM $Mg(OAc)_2$ [pH 7.4]) in the presence of ATP (5 mM) and an ATP regeneration system (0.1 mM ATP, 0.02 mg/ml creatine kinase, 10 mM creatine phosphate). Samples were incubated at 37°C for the duration of the experiments. At various time points, aliquots were removed and analyzed. For ThT fluorescence measurements, samples were added to a 96-well plate containing 25 μM ThT diluted in assay buffer. Changes in fluorescence intensity (excitation 440 nm, 5 nm bandwidth; emission 482 nm, 10 nm bandwidth) were measured using a Tecan Safire^2 microplate reader.

TEM

For TEM, reaction aliquots were spotted on Formvar carbon-coated grids (EM Sciences) and stained with 2% uranyl acetate. Samples were visualized using a JEOL-1010 electron microscope.

Filter Trap

Reactions were centrifuged in Microcon centrifugal filter devices (Amicon) for 25 min at 14,000 relative centrifugal force. Filtrate and retentate fractions were analyzed by SDS-PAGE using 10%–20% Tris-Tricine peptide gels (Bio-Rad). Gels were visualized by silver staining (Invitrogen).

Turbidity

Fibrils (20 μM monomer) were incubated with the indicated concentrations of Hsp104 variants, and diluted into assay buffer in the presence of ATP (5 mM) and an ATP regeneration system (0.1 mM ATP, 0.02 mg/ml creatine kinase, 10 mM creatine phosphate). Turbidity was measured as absorbance at 395 nm at room temperature on a Tecan Safire^2 microplate reader.

DLS

SEVI fibrils (20 μM monomer) were incubated for ~5 min with the indicated proteins (1.8 μM monomeric concentration) and diluted into assay buffer in the presence of ATP (5 mM). Samples were immediately transferred into disposable cuvettes (Eppendorf) and light scattering at 658 nm was measured using a DynaPro NanoStar DLS instrument (Wyatt Technology). DLS measurements of R_h were made at room temperature. Samples were measured using an acquisition time of 10 s for ten consecutive measurements. Particle translational diffusion coefficients were calculated from decay curves of autocorrelation of light-scattering data and converted to R_h with the Stokes-Einstein equation. Histograms of mass versus R_h were calculated using a Regularization algorithm with Dynamics V7 software.

Fibril Degradation

Fibrils (20 μM monomer) were incubated with HAP (3 μM) and ClpP (4.5 μM), and diluted into an assay buffer in the presence of ATP and an ATP regeneration system (as above). Samples were incubated at 37°C for the duration of the experiments. At given time points, aliquots were removed and analyzed by SDS-PAGE on peptide gels followed by silver staining (Invitrogen).

Cell Culture and HIV Infection

TZM-bl cells were maintained in DMEM supplemented with 10% fetal bovine serum and 1% L-glutamine. Prior to infection, seminal amyloid fibrils were incubated with Hsp104 (or variants) in a sterile reaction tube for 3 hr at 37°C. Next, these mixtures were diluted 1:2 in DMEM, followed by a subsequent 1:2 dilution with HIV-1. Samples were allowed to preincubate with the virus for 10 min at room temperature. The virus/protein mixtures were added in triplicate to TZM-bl cells (10^4 cells/well) and incubated for 3 hr at 37°C and 5% CO_2. Virus/protein mixtures were then removed and replaced with 200 μl of complete media. Luciferase activity was assessed 3 days after infection using a Luciferase Assay System (Promega), and luminescence was measured on an MLX Microtiter Plate Luminometer (Dynex Technologies). Background luminescence from buffer control samples was subtracted and values were normalized to untreated fibril samples. HIV-1 strains used included BL2 (CCR5 using primary isolate; 65 infectious units; 0.45 ng p24) and 89.6 (dual tropic; 500 infectious units; 0.46 ng p24).

Analysis of Cellular Toxicity

Cell viability of TZM-bl cells treated with Hsp104 or variants was also measured using the 3-(4,5-dimethylthiazol-2-yl)-2,5-diphenyltetrazolium bromide (MTT) reduction assay. TZM-bl cells (10^4 cells/well) were treated as described in the HIV infectivity assays, except with DMEM replacing virus at each step. Protein/DMEM mixtures were removed after 3 hr and replaced with 200 μl of complete media. Plates were incubated overnight at 37°C. The next day, an MTT stock (50 mg of MTT dissolved in 10 ml of PBS) was mixed in a 1:1 ratio with DMEM to result in the MTT reagent. Media were removed from all wells on the 96-well plate and replaced with 125 μl of fresh media. MTT reagent (25 μl) was added to each well and incubated at 37°C for 3–4 hr. Formazan crystals were dissolved in 150 μl of 0.1 N HCl in isopropanol with 10% Triton X-100. MTT reduction was assessed the by detection of absorbance at 570 nm (630 nm reference wavelength) on an MRX Revelation Microplate Reader (Dynex Technologies).

SUPPLEMENTAL INFORMATION

Supplemental Information includes five figures and can be found with this article online at http://dx.doi.org/10.1016/j.chembiol.2015.07.007.

ACKNOWLEDGMENTS

We thank Walid Houry and Sue Lindquist for generous provision of reagents; Rebecca Hammond for assistance with SEM1(45–107) fibrils; Onofrio Zirafi and Jan Münch for preliminary experiments; Meredith Jackrel, Mariana Torrente, Lin Guo, Alice Ford, and Korrie Mack for critiques; and Shorter lab members for helpful suggestions. Our work was supported by an NSF Graduate Research Fellowship DGE-0822 (L.M.C.); a Bill and Melinda Gates Foundation Grand Challenges Explorations Award, a Linda Pechenik Montague Investigator Award, and NIH grants DP2OD002177, R01GM099836, and R21HD074510 (J.S.).

Received: November 25, 2014
Revised: June 30, 2015
Accepted: July 7, 2015
Published: August 6, 2015

REFERENCES

Amen, T., and Kaganovich, D. (2015). Dynamic droplets: the role of cytoplasmic inclusions in stress, function, and disease. Cell. Mol. Life Sci. *72*, 401–415.

Arnold, F., Schnell, J., Zirafi, O., Sturzel, C., Meier, C., Weil, T., Standker, L., Forssmann, W.G., Roan, N.R., Greene, W.C., et al. (2012). Naturally occurring fragments from two distinct regions of the prostatic acid phosphatase form amyloidogenic enhancers of HIV infection. J. Virol. *86*, 1244–1249.

Barnett, M.E., Nagy, M., Kedzierska, S., and Zolkiewski, M. (2005). The amino-terminal domain of ClpB supports binding to strongly aggregated proteins. J. Biol. Chem. *280*, 34940–34945.

Bosl, B., Grimminger, V., and Walter, S. (2005). Substrate binding to the molecular chaperone Hsp104 and its regulation by nucleotides. J. Biol. Chem. *280*, 38170–38176.

Brender, J.R., Nanga, R.P., Popovych, N., Soong, R., Macdonald, P.M., and Ramamoorthy, A. (2011). The amyloidogenic SEVI precursor, PAP248-286, is highly unfolded in solution despite an underlying helical tendency. Biochim. Biophys. Acta *1808*, 1161–1169.

Cashikar, A.G., Schirmer, E.C., Hattendorf, D.A., Glover, J.R., Ramakrishnan, M.S., Ware, D.M., and Lindquist, S.L. (2002). Defining a pathway of communication from the C-terminal peptide binding domain to the N-terminal ATPase domain in a AAA protein. Mol. Cell *9*, 751–760.

Castellano, L.M., and Shorter, J. (2012). The surprising role of amyloid fibrils in HIV infection. Biology *1*, 58–80.

Cushman, M., Johnson, B.S., King, O.D., Gitler, A.D., and Shorter, J. (2010). Prion-like disorders: blurring the divide between transmissibility and infectivity. J. Cell Sci. *123*, 1191–1201.

Cushman-Nick, M., Bonini, N.M., and Shorter, J. (2013). Hsp104 suppresses polyglutamine-induced degeneration post onset in a *Drosophila* MJD/SCA3 model. PLoS Genet. *9*, e1003781.

DeSantis, M.E., and Shorter, J. (2012a). The elusive middle domain of Hsp104 and ClpB: location and function. Biochim. Biophys. Acta *1823*, 29–39.

DeSantis, M.E., and Shorter, J. (2012b). Hsp104 drives "protein-only" positive selection of Sup35 prion strains encoding strong [PSI(+)]. Chem. Biol. *19*, 1400–1410.

DeSantis, M.E., Leung, E.H., Sweeny, E.A., Jackrel, M.E., Cushman-Nick, M., Neuhaus-Follini, A., Vashist, S., Sochor, M.A., Knight, M.N., and Shorter, J. (2012). Operational plasticity enables Hsp104 to disaggregate diverse amyloid and nonamyloid clients. Cell *151*, 778–793.

DeSantis, M.E., Sweeny, E.A., Snead, D., Leung, E.H., Go, M.S., Gupta, K., Wendler, P., and Shorter, J. (2014). Conserved distal loop residues in the Hsp104 and ClpB middle domain contact nucleotide-binding domain 2 and enable Hsp70-dependent protein disaggregation. J. Biol. Chem. *289*, 848–867.

Glover, J.R., and Lindquist, S. (1998). Hsp104, Hsp70, and Hsp40: a novel chaperone system that rescues previously aggregated proteins. Cell *94*, 73–82.

Gray, R.H., Wawer, M.J., Brookmeyer, R., Sewankambo, N.K., Serwadda, D., Wabwire-Mangen, F., Lutalo, T., Li, X., vanCott, T., Quinn, T.C., et al. (2001). Probability of HIV-1 transmission per coital act in monogamous, heterosexual, HIV-1-discordant couples in Rakai, Uganda. Lancet *357*, 1149–1153.

Hattendorf, D.A. (2001). Multiple Allosteric Signaling Events in the Hsp104 ATP Hydrolysis Cycle Revealed by Mutagenesis of Conserved AAA Active Site Residues (University of Chicago, Department of Biochemistry and Molecular Biology).

Hauber, I., Hohenberg, H., Holstermann, B., Hunstein, W., and Hauber, J. (2009). The main green tea polyphenol epigallocatechin-3-gallate counteracts semen-mediated enhancement of HIV infection. Proc. Natl. Acad. Sci. USA *106*, 9033–9038.

Jackrel, M.E., and Shorter, J. (2014). Potentiated Hsp104 variants suppress toxicity of diverse neurodegenerative disease-linked proteins. Dis. Model. Mech. *7*, 1175–1184.

Jackrel, M.E., and Shorter, J. (2015). Engineering enhanced protein disaggregases for neurodegenerative disease. Prion *9*, 90–109.

Jackrel, M.E., DeSantis, M.E., Martinez, B.A., Castellano, L.M., Stewart, R.M., Caldwell, K.A., Caldwell, G.A., and Shorter, J. (2014). Potentiated Hsp104 variants antagonize diverse proteotoxic misfolding events. Cell *156*, 170–182.

Kim, Y., Park, J.H., Jang, J.Y., Rhim, H., and Kang, S. (2013). Characterization and Hsp104-induced artificial clearance of familial ALS-related SOD1 aggregates. Biochem. Biophys. Res. Commun. *434*, 521–526.

Klaips, C.L., Hochstrasser, M.L., Langlois, C.R., and Serio, T.R. (2014). Spatial quality control bypasses cell-based limitations on proteostasis to promote prion curing. Elife *3*, e04288.

Knowles, T.P., Vendruscolo, M., and Dobson, C.M. (2014). The amyloid state and its association with protein misfolding diseases. Nat. Rev. Mol. Cell Biol. *15*, 384–396.

Liu, Y.H., Han, Y.L., Song, J., Wang, Y., Jing, Y.Y., Shi, Q., Tian, C., Wang, Z.Y., Li, C.P., Han, J., et al. (2011). Heat shock protein 104 inhibited the fibrillization of prion peptide 106-126 and disassembled prion peptide 106-126 fibrils in vitro. Int. J. Biochem. Cell Biol. *43*, 768–774.

Lo Bianco, C., Shorter, J., Regulier, E., Lashuel, H., Iwatsubo, T., Lindquist, S., and Aebischer, P. (2008). Hsp104 antagonizes alpha-synuclein aggregation and reduces dopaminergic degeneration in a rat model of Parkinson disease. J. Clin. Invest. *118*, 3087–3097.

Lum, R., Niggemann, M., and Glover, J.R. (2008). Peptide and protein binding in the axial channel of Hsp104. Insights into the mechanism of protein unfolding. J. Biol. Chem. *283*, 30139–30150.

Mannini, B., Cascella, R., Zampagni, M., van Waarde-Verhagen, M., Meehan, S., Roodveldt, C., Campioni, S., Boninsegna, M., Penco, A., Relini, A., et al. (2012). Molecular mechanisms used by chaperones to reduce the toxicity of aberrant protein oligomers. Proc. Natl. Acad. Sci. USA *109*, 12479–12484.

Münch, J., Rucker, E., Standker, L., Adermann, K., Goffinet, C., Schindler, M., Wildum, S., Chinnadurai, R., Rajan, D., Specht, A., et al. (2007). Semen-derived amyloid fibrils drastically enhance HIV infection. Cell *131*, 1059–1071.

Narayanan, S., Bosl, B., Walter, S., and Reif, B. (2003). Importance of low-oligomeric-weight species for prion propagation in the yeast prion system Sup35/Hsp104. Proc. Natl. Acad. Sci. USA *100*, 9286–9291.

Oguchi, Y., Kummer, E., Seyffer, F., Berynskyy, M., Anstett, B., Zahn, R., Wade, R.C., Mogk, A., and Bukau, B. (2012). A tightly regulated molecular toggle controls AAA+ disaggregase. Nat. Struct. Mol. Biol. *19*, 1338–1346.

Olsen, J.S., DiMaio, J.T., Doran, T.M., Brown, C., Nilsson, B.L., and Dewhurst, S. (2012). Seminal plasma accelerates semen-derived enhancer of viral infection (SEVI) fibril formation by the prostatic acid phosphatase (PAP248-286) peptide. J. Biol. Chem. *287*, 11842–11849.

Pilcher, C.D., Tien, H.C., Eron, J.J., Jr., Vernazza, P.L., Leu, S.Y., Stewart, P.W., Goh, L.E., Cohen, M.S., Quest Study, and Duke-UNC-Emory Acute HIV Consortium. (2004). Brief but efficient: acute HIV infection and the sexual transmission of HIV. J. Infect. Dis. *189*, 1785–1792.

Roan, N.R., Münch, J., Arhel, N., Mothes, W., Neidleman, J., Kobayashi, A., Smith-McCune, K., Kirchhoff, F., and Greene, W.C. (2009). The cationic properties of SEVI underlie its ability to enhance human immunodeficiency virus infection. J. Virol. *83*, 73–80.

Roan, N.R., Muller, J.A., Liu, H., Chu, S., Arnold, F., Sturzel, C.M., Walther, P., Dong, M., Witkowska, H.E., Kirchhoff, F., et al. (2011). Peptides released by physiological cleavage of semen coagulum proteins form amyloids that enhance HIV infection. Cell Host Microbe *10*, 541–550.

Royce, R.A., Sena, A., Cates, W., Jr., and Cohen, M.S. (1997). Sexual transmission of HIV. N. Engl. J. Med. *336*, 1072–1078.

Shorter, J. (2008). Hsp104: a weapon to combat diverse neurodegenerative disorders. Neurosignals *16*, 63–74.

Shorter, J. (2011). The mammalian disaggregase machinery: Hsp110 synergizes with Hsp70 and Hsp40 to catalyze protein disaggregation and reactivation in a cell-free system. PLoS One *6*, e26319.

Shorter, J., and Lindquist, S. (2004). Hsp104 catalyzes formation and elimination of self-replicating Sup35 prion conformers. Science *304*, 1793–1797.

Shorter, J., and Lindquist, S. (2005). Navigating the ClpB channel to solution. Nat. Struct. Mol. Biol. *12*, 4–6.

Shorter, J., and Lindquist, S. (2006). Destruction or potentiation of different prions catalyzed by similar Hsp104 remodeling activities. Mol. Cell *23*, 425–438.

Shorter, J., and Lindquist, S. (2008). Hsp104, Hsp70 and Hsp40 interplay regulates formation, growth and elimination of Sup35 prions. EMBO J. *27*, 2712–2724.

Sievers, S.A., Karanicolas, J., Chang, H.W., Zhao, A., Jiang, L., Zirafi, O., Stevens, J.T., Münch, J., Baker, D., and Eisenberg, D. (2011). Structure-based design of non-natural amino-acid inhibitors of amyloid fibril formation. Nature *475*, 96–100.

Sweeny, E.A., and Shorter, J. (2008). Prion proteostasis: Hsp104 meets its supporting cast. Prion *2*, 135–140.

Sweeny, E.A., Jackrel, M.E., Go, M.S., Sochor, M.A., Razzo, B.M., DeSantis, M.E., Gupta, K., and Shorter, J. (2015). The Hsp104 N-terminal domain enables disaggregase plasticity and potentiation. Mol. Cell *57*, 836–849.

Tessarz, P., Mogk, A., and Bukau, B. (2008). Substrate threading through the central pore of the Hsp104 chaperone as a common mechanism for protein disaggregation and prion propagation. Mol. Microbiol. *68*, 87–97.

UNAIDS. (2010). Global Report: UNAIDS Report on the Global AIDS Epidemic 2010 (Joint United Nations Programme on HIV/AIDS (UNAIDS)), pp. 1–359.

UNAIDS. (2011). World AIDS Day Report 2011 (Joint United Nations Programme on HIV/AIDS (UNAIDS)), pp. 1–48.

Usmani, S.M., Zirafi, O., Muller, J.A., Sandi-Monroy, N.L., Yadav, J.K., Meier, C., Weil, T., Roan, N.R., Greene, W.C., Walther, P., et al. (2014). Direct visualization of HIV-enhancing endogenous amyloid fibrils in human semen. Nat. Commun. *5*, 3508.

Vashist, S., Cushman, M., and Shorter, J. (2010). Applying Hsp104 to protein-misfolding disorders. Biochem. Cell Biol. *88*, 1–13.

Wang, J., Hartling, J.A., and Flanagan, J.M. (1997). The structure of ClpP at 2.3 A resolution suggests a model for ATP-dependent proteolysis. Cell *91*, 447–456.

Ye, Z., French, K.C., Popova, L.A., Lednev, I.K., Lopez, M.M., and Makhatadze, G.I. (2009). Mechanism of fibril formation by a 39-residue peptide (PAPf39) from human prostatic acidic phosphatase. Biochemistry *48*, 11582–11591.

Yolamanova, M., Meier, C., Shaytan, A.K., Vas, V., Bertoncini, C.W., Arnold, F., Zirafi, O., Usmani, S.M., Muller, J.A., Sauter, D., et al. (2013). Peptide nanofibrils boost retroviral gene transfer and provide a rapid means for concentrating viruses. Nat. Nanotechnol. *8*, 130–136.

Yu, A.Y., and Houry, W.A. (2007). ClpP: a distinctive family of cylindrical energy-dependent serine proteases. FEBS Lett. *581*, 3749–3757.

Chemistry & Biology, Volume *22*

Supplemental Information

Repurposing Hsp104 to Antagonize Seminal Amyloid and Counter HIV Infection

Laura M. Castellano, Stephen M. Bart, Veronica M. Holmes, Drew Weissman, and James Shorter

Figure S1. Hsp104 and Hsp104^{A503V} rapidly remodel PAP85- fibrils, Related to Figure 1 and 2. (A) Preformed PAP85-120 fibrils (20μM monomer) were incubated with buffer (untreated), Hsp104, Hsp104^{DWB}, or ClpB (3μM) for 0-24h. Fibril integrity was assessed via ThT fluorescence. Values represent means ± SEM (n=3-7). **(B)** TEM of PAP85-120 fibrils incubated with buffer (untreated) or Hsp104 (3μM) for 6h. The scale bar is indicated. **(C)** Preformed PAP85-120 fibrils (20μM monomer) were incubated with buffer (untreated) or Hsp104^{A503V} (3μM) for 0-24h. Fibril integrity was assessed via ThT fluorescence. Values represent means ± SEM (n=4). **(D)** TEM of PAP85-120 fibrils incubated with buffer (untreated) or Hsp104^{A503V} (3μM) for 6h. The scale bar is indicated.

Figure S2. Hsp104 and Hsp104^{A503V} do not remodel SEM1(45-107) fibrils, Related to Figure 1 and 2. (A) Preformed SEM1(45-107) fibrils (20μM monomer) were incubated with buffer (untreated), Hsp104, Hsp104^{DWB} or ClpB (3μM) for 0-24h. Fibril integrity was assessed via ThT fluorescence. Values represent means ± SEM (n=3). **(B)** TEM of SEM1(45-107) fibrils incubated with buffer (untreated) or Hsp104 (3μM) for 6h. The scale bar is indicated. **(C)** Preformed SEM1(45-107) fibrils (20μM monomer) were incubated with buffer (untreated) or Hsp104^{A503V} (3μM) for 0-24h. Fibril integrity was assessed via ThT fluorescence. Values represent means ± SEM (n=3). **(D)** TEM of SEM1(45-107) fibrils incubated with buffer (untreated) or Hsp104^{A503V} (3μM) for 6h. The scale bar is indicated.

Figure S3. ClpB and monomeric Hsp104$^{1-548}$ promote clustering of seminal amyloid fibrils, Related to Figure 3. (A-C) SEVI **(A)**, PAP85-120 **(B)**, and SEM1(45-107) **(C)** fibrils (20μM monomer) were incubated with buffer (untreated) or ClpB (1.8μM monomer) and absorbance at 395nm was measured continuously for 3h. One representative trial is shown. **(D-E)** PAP85-120 **(D)** or SEM1(45-107) **(E)** fibrils (20μM monomer) were incubated with buffer (untreated), Hsp104$^{1-548}$, or Hsp104$^{773-908}$ (1.8μM monomer) and absorbance at 395nm was measured continuously for 3h. One representative trial is shown.

Figure S4. Size distribution of Hsp104 and soluble PAP248-286, Related to Figure 3. (A, B) Dynamic light scattering was used to determine the hydrodynamic radius (R_h) of Hsp104 (0.3μM hexamer) **(A)** and soluble PAP248-286 (20μM) **(B)**.

Figure S5. Hsp104$^{871-908}$ does not affect the ability of SEVI fibrils to promote HIV infection, , Related to Figure 5. SEVI fibrils (20μM) were pretreated with buffer or Hsp104$^{871-908}$ (18μM) and HIV infectivity was assessed in TZM-bl cells and expressed as normalized infectivity. Values represent means ± SEM (n=2).

Figure S1

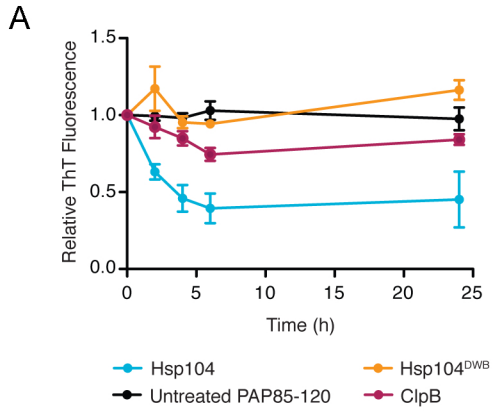
A
Relative ThT Fluorescence
1.5
1.0
0.5
0.0
0
5
10
15
20
25
Time (h)
Hsp104
Hsp104DWB
Untreated PAP85-120
ClpB

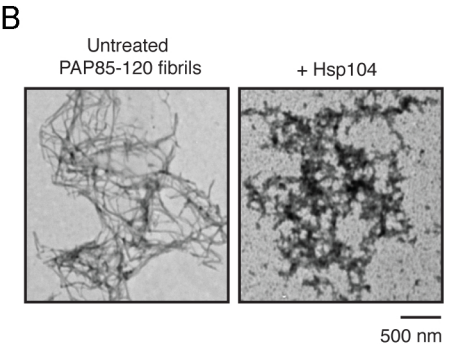
B
Untreated
PAP85-120 fibrils
+ Hsp104
500 nm

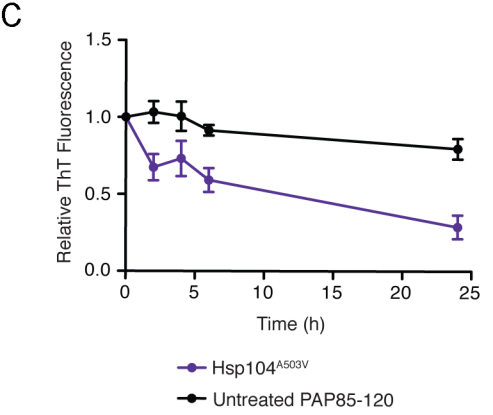
C
Relative ThT Fluorescence
1.5
1.0
0.5
0.0
0
5
10
15
20
25
Time (h)
Hsp104A503V
Untreated PAP85-120

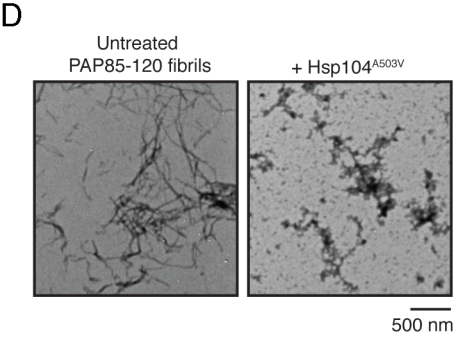
D
Untreated
PAP85-120 fibrils
+ Hsp104A503V
500 nm

Figure S2

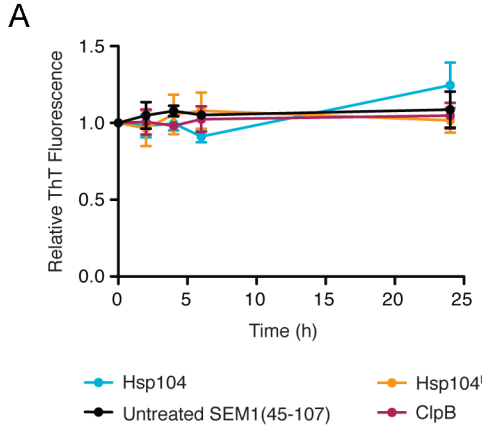
A
Relative ThT Fluorescence
1.5
1.0
0.5
0.0
0
5
10
15
20
25
Time (h)
Hsp104
Untreated SEM1(45-107)
Hsp104DWB
ClpB

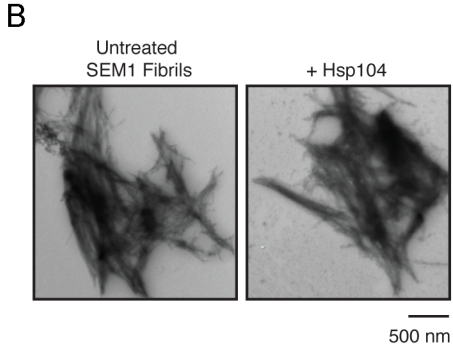
B
Untreated
SEM1 Fibrils
+ Hsp104
500 nm

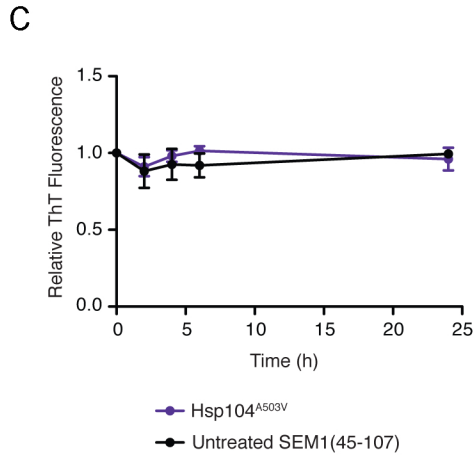
C
Relative ThT Fluorescence
1.5
1.0
0.5
0.0
0
5
10
15
20
25
Time (h)
Hsp104A503V
Untreated SEM1(45-107)

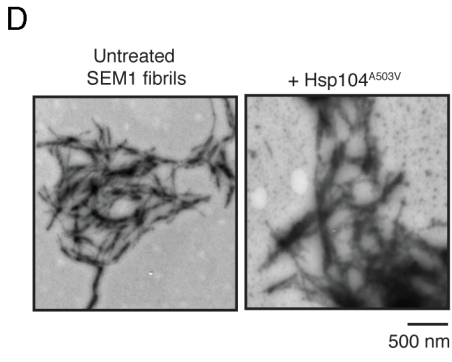
D
Untreated
SEM1 fibrils
+ Hsp104A503V
500 nm

Figure S3

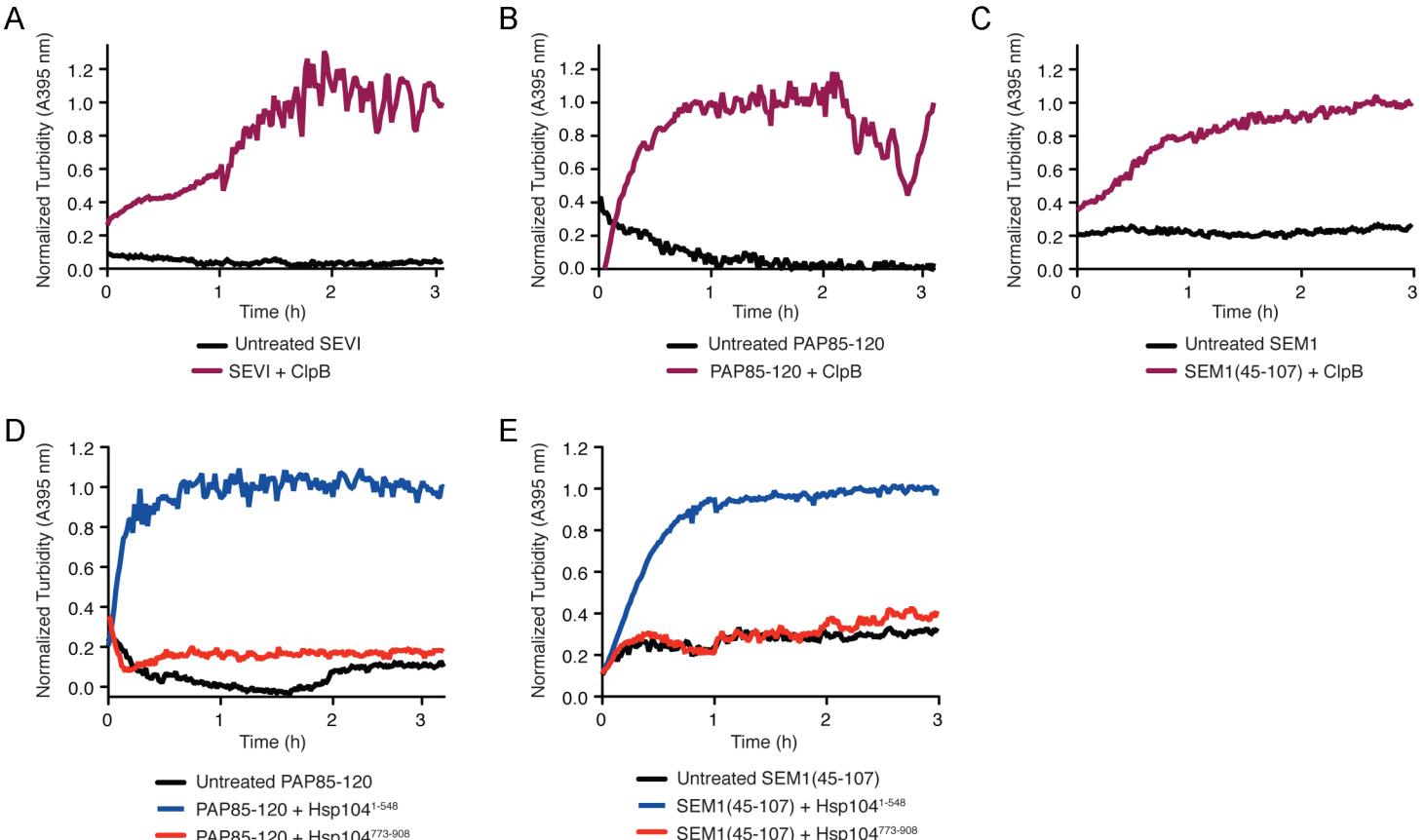
A
Normalized Turbidity (A395 nm)
Time (h)
Untreated SEVI
SEVI + ClpB
B
Normalized Turbidity (A395 nm)
Time (h)
Untreated PAP85-120
PAP85-120 + ClpB
C
Normalized Turbidity (A395 nm)
Time (h)
Untreated SEM1
SEM1(45-107) + ClpB
D
Normalized Turbidity (A395 nm)
Time (h)
Untreated PAP85-120
PAP85-120 + Hsp104 1-548
PAP85-120 + Hsp104 773-908
E
Normalized Turbidity (A395 nm)
Time (h)
Untreated SEM1(45-107)
SEM1(45-107) + Hsp104 1-548
SEM1(45-107) + Hsp104 773-908

Figure S4

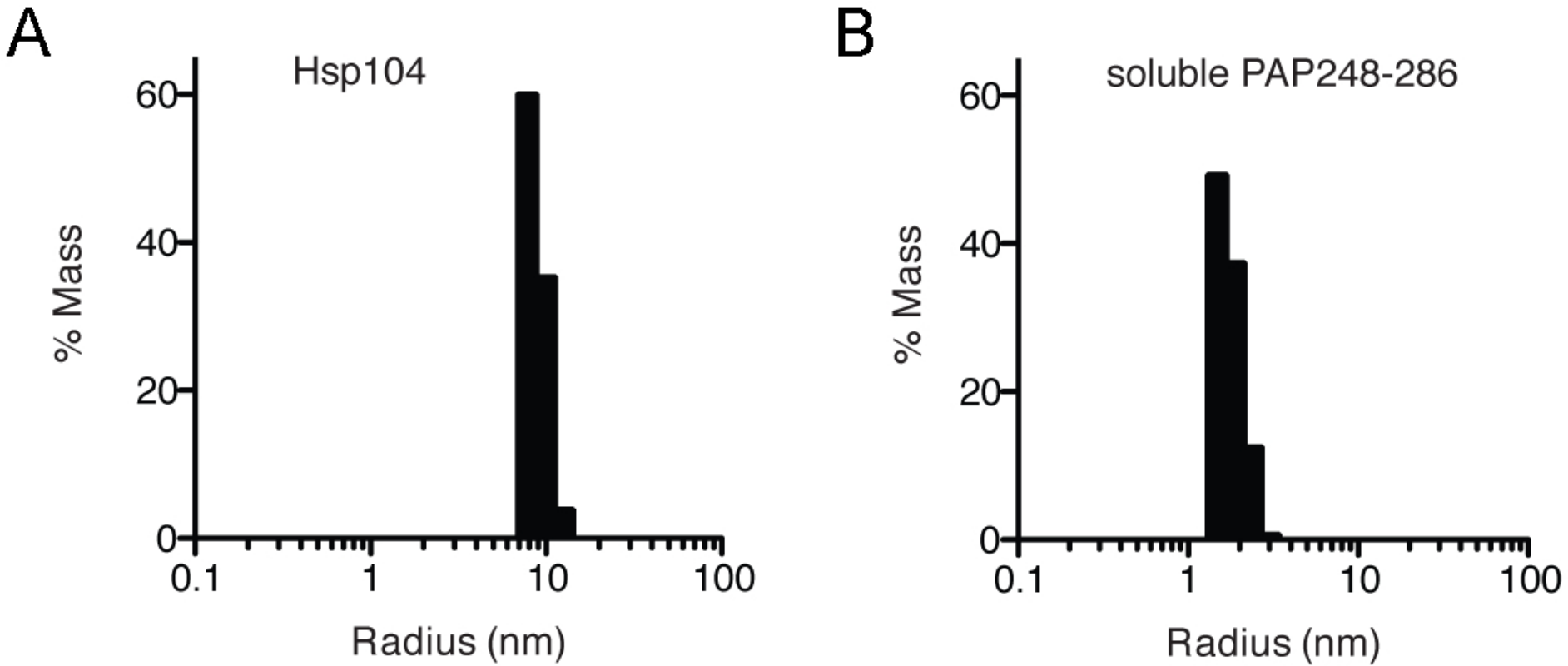
A
Hsp104
60
40
20
0
% Mass
0.1
1
10
100
Radius (nm)
B
soluble PAP248-286
60
40
20
0
% Mass
0.1
1
10
100
Radius (nm)

Figure S5.

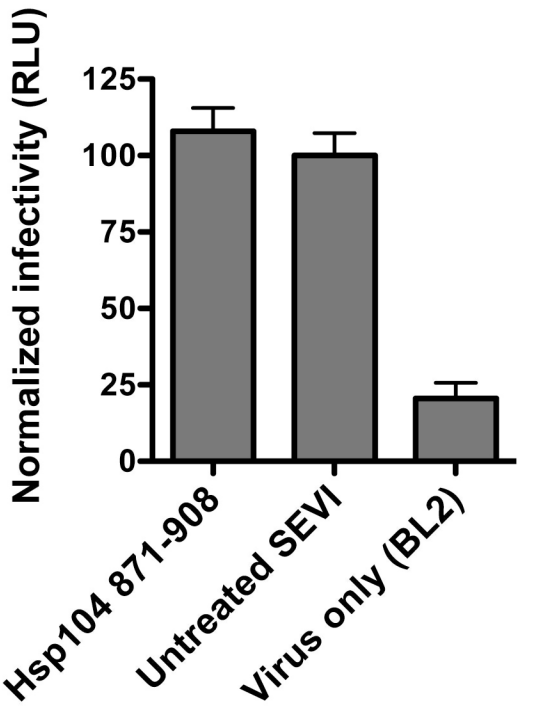
Normalized infectivity (RLU)
125
100
75
50
25
0
Hsp104 871-908
Untreated SEVI
Virus only (BL2)